Light and stable triplet bipolarons on square and triangular lattices

J. P. Hague

Department of Physics and Astronomy, The Open University, Walton Hall, Milton Keynes MK7 6AA, United Kingdom

P. E. Kornilovitch

Hewlett-Packard Company, 1000 NE Circle Boulevard, Corvallis, Oregon 97330, USA

(Received 7 October 2009; revised manuscript received 5 July 2010; published 1 September 2010)

We compute the properties of singlet and triplet bipolarons on two-dimensional lattices using the continuous-time quantum Monte Carlo algorithm. Properties of the bipolaron including the total energy, inverse mass, bipolaron radius, and number of phonons associated with the bipolaron demonstrate the qualitative difference between models of electron-phonon interaction with long-range interaction (screened Fröhlich) and those with purely local (Holstein) interaction. A major result of our survey of the parameter space is the existence of extra-light hybrid singlet bipolarons consisting of an on-site and an off-site component on both square and triangular lattices. We also compute triplet properties of the bipolarons and the pair dispersion. For pair momenta on the edge of the Brillouin zone of the triangular lattice, we find that triplet states are more stable than singlets.

I. INTRODUCTION

A fascinating scenario for phonon-mediated superconductivity involves the pairing of polarons into bipolarons at strong electron-phonon coupling.[1] If the resulting pairs are sufficiently small that the bipolarons are well separated relative to their size, then the pairs act like bosons and a Bose-Einstein condensate (BEC) of bipolarons could form. The transition temperature of such a condensate is limited by properties such as the mass and size of the pairs. Therefore, to examine the possibility of such a scenario at observable temperatures, it is essential to have good data regarding bipolaron properties. It is the purpose of this paper to use the numerically exact continuous-time quantum Monte Carlo (CTQMC) algorithm to make a comprehensive survey of the properties of Hubbard-Fröhlich bipolarons on both triangular and square lattices.

There are a number of exact numerical methods for studying bipolaron formation in one-dimensional (1D) systems with electron-phonon interactions such as exact-diagonalization (ED),[2,3] advanced variational techniques,[4] density-matrix renormalization-group (DMRG),[5] and various QMC approaches.[6–8] In two-dimensional (2D) systems, many of those techniques are not applicable. Exact diagonalization cannot cope with large numbers of lattice sites, DMRG schemes are not easy to develop in 2D, and both ED and DMRG can suffer from a truncation of the phonon Hilbert space, rendering those methods inefficient at strong electron-phonon coupling. Also, the Hilbert space of advanced variational techniques grows too fast for application to 2D bipolarons (although we note that the technique can be applied to polarons in three dimensions without problems[9]). On the other hand, QMC techniques (and especially continuous-time QMC) can cope with large lattice sizes and treat the phonon degrees of freedom exactly, making them well suited for computations of bipolarons on two- and potentially even three-dimensional lattices.

There is an interesting possibility relating to bipolarons in 2D. If a lattice is made up from triangular plaquettes, and if

there is a strong Coulomb repulsion keeping bipolarons from pairing on-site, superlight small bipolarons can form.[10–13] Our aim here is to comprehensively compute the properties of bipolarons with long-range interaction on both square and triangular lattices to determine if there are any other promising ways that bipolarons can pair. The Hubbard-Holstein bipolaron on the square lattice was studied by Macridin *et al.*[14] using the related diagrammatic quantum Monte Carlo technique. Bipolaron formation in the Hubbard-Holstein model has also been studied approximately in 1D (Ref. 15) and in 2D on the square lattice[16] using variational methods leading to qualitatively similar results. Our current study goes beyond this previous work by computing the properties of bipolarons formed from long-range electron-phonon interactions. We also compute properties of bipolarons on triangular lattices, which have not been comprehensively studied even for the Holstein interaction. Our CTQMC algorithm is particularly efficient for this task since phonon degrees of freedom can be treated exactly to generate an effective retarded interaction between electrons.

In this paper, we study the screened Hubbard-Fröhlich model, which has the Hamiltonian,

$$
H = -t \sum_{\langle nn'\rangle\sigma} c^\dagger_{n'\sigma} c_{n\sigma} + U \sum_n c^\dagger_{n\uparrow} c_{n\uparrow} c^\dagger_{n\downarrow} c_{n\downarrow} + \sum_m \frac{\hat{P}^2_m}{2M}
$$
$$
+ \sum_m \frac{\xi^2_m M \omega^2}{2} - \sum_{nm\sigma} f_m(n) c^\dagger_{n\sigma} c_{n\sigma} \xi_m. \tag{1}
$$

Here, $c^\dagger_n$ creates an electron on site n, t is the intersite hopping integral, U is the Hubbard repulsion, M is the ion mass, ω is the ion oscillation frequency, ξ is the ion displacement, and $\hat{P}$ is the ion momentum. The electron-ion force function is f and has the form $f_m(n) = \kappa[(m-n)^2+1]^{-3/2}\exp(-|m-n|/R_{sc})$. The screening radius R_{sc} controls the length of the interaction and κ is the strength of the interaction. m represents the position of the ion and n is the position of the

electron. The electron-ion interaction leads to an effective retarded electron-electron interaction characterized by the function,

$$\Phi_{\Delta r}[r(\tau), r(\tau')] = \sum_m f_m[r(\tau)] f_{m+\Delta r}[r(\tau')], \quad (2)$$

where Δr is the offset between end configurations of the paths (see Sec. II). By changing R_{sc} it is possible to investigate the Hubbard-Holstein model ($R_{sc} \to 0$) and the Hubbard-Fröhlich model ($R_{sc} \to \infty$). We also consider a model similar to the nearest-neighbor model of Bonča and Trugman,[17] where effective electron-electron interactions are truncated at near-neighbor sites [$\Phi(a) = \Phi(0)/2$ and all other $\Phi = 0$, where a are vectors to the near-neighbor sites]. This simplified model maps directly onto a U-V model in the large phonon frequency limit and could be particularly useful for understanding limiting behavior.[18]

This paper is structured as follows. In Sec. II, we briefly review the differences between the CTQMC algorithm in 1D and 2D. In Secs. III and IV we make a comprehensive survey of the parameter space of singlet bipolarons in 2D. Triplet properties are discussed in Sec. V. One of the additional advantages of our algorithm is that bipolaron dispersions can be computed efficiently, especially in the large λ regime, and these are shown in Sec. VI. Finally we summarize in Sec. VII.

II. METHOD

We use a continuous-time quantum Monte Carlo algorithm based on path integrals. We have previously discussed our algorithm in detail with regard to computations in 1D,[6] so we do not repeat those details here. To aid the reader of this section, we briefly recap some of our terminology: we have two paths, which are configurations forming the integrand of a path integral, where each path represents a single particle and exists on the imaginary time interval $\tau \in [0, \beta]$. Our Monte Carlo procedure performs the path integral by probing different path configurations which each have a weight $\exp(A)$, where A is the action of the configuration given by

$$A[r_1, r_2] = \frac{z\lambda\bar{\omega}}{2\Phi_0(0,0)} \int_0^{\bar{\beta}} \int_0^{\bar{\beta}} d\tau d\tau' e^{-\bar{\omega}\bar{\beta}/2} (e^{\bar{\omega}(\bar{\beta}/2 - |\tau - \tau'|)}$$
$$+ e^{-\bar{\omega}(\bar{\beta}/2 - |\tau - \tau'|)}) \sum_{ij} \Phi_0[r_i(\tau), r_j(\tau')]$$
$$+ \frac{z\lambda\bar{\omega}}{\Phi_0(0,0)} \int_0^{\bar{\beta}} \int_0^{\bar{\beta}} d\tau d\tau' e^{-\bar{\omega}\tau} e^{-\bar{\omega}(\bar{\beta} - \tau')}$$
$$\times \sum_{ij} (\Phi_{\Delta r}[r_i(\tau), r_j(\tau')] - \Phi_0[r_i(\tau), r_j(\tau')])$$
$$- \int_0^\beta V[r_1(\tau), r_2(\tau)] d\tau \quad (3)$$

(note the sign convention). The symbols $\bar{\beta} = t/T$, $\bar{\omega} = \omega/t$, and $V(r_1, r_2)$ is the instantaneous electrostatic interaction between electrons and for the Hubbard interaction has the form

$V(r_1, r_2) = U\delta_{r_1, r_2}$, z is the coordination number and $\lambda = E_p/zt$, where $E_p = \Phi_0(0,0)/2M\omega^2$ is the polaron shift. Paths are formed from straight segments, punctuated with kinks that correspond to hopping from one site to another. A schematic showing example paths can be found in several of our papers. Path configurations are updated via a Metropolis procedure to perform the path integral. In order to compute the effective mass and dispersion, the boundary conditions in time are "twisted" so that there is an offset Δr between the ends of the paths at times $\tau = 0$ and $\tau = \beta$.[6] This twisting of the boundary conditions leads to the second term in the action.

There are a few small subtleties relating to using the algorithm in 2D, especially on a triangular lattice, which are discussed below. Our algorithm has been thoroughly checked against results from the U-V model, which represents the large phonon frequency limit of the near-neighbor interaction. We also checked against exactly known results for bipolarons in 1D (Ref. 19) and against diagrammatic quantum Monte Carlo.[20] Details of code checks can be found in Appendices A and B.

A. Triple kink insertions on triangular lattices

The algorithm is subtly different on triangular lattices or more generally on any lattice where an electron can return to its original position in three hops (such as lattices with nearest- and next-nearest-neighbor hoppings). We illustrate this by considering an example configuration that is permitted on such lattices: let one of the paths have no kinks while the other path has three kinks—one in each of the nearest-neighbor directions—so that the start and end of each path lies on the same lattice site. Such a configuration is clearly permitted since the periodic boundary conditions in imaginary time are satisfied. However, if only binary kink insertions are included in the algorithm then it is not possible to update between configurations with odd and even numbers of kinks. Thus, to ensure ergodicity, an update with a three-kink insertion is proposed.

Our scheme for three-kink insertion is similar to the one that we use for binary updates. To avoid complications, we do not weight the positions of the kinks in imaginary time. Ternary kink insertions do not need to be especially efficient; if path configurations can be updated from even to odd numbers of kinks (and vice versa) with reasonable regularity, binary insertions can be used to sample the remaining configurations efficiently. Our scheme is as follows: (1) we select a kink type from the six possible kinks and assign the label l_1. (2) We choose kinks at 120° and 240° rotations from l_1 and assign them the labels l_2 and l_3. (3) We choose insertion or removal of kinks with equal probability 1/2. (4) If inserting, we choose imaginary times τ_1, τ_2, and τ_3 for the new kinks with equal probability $1/\beta$ from the interval $[1, \beta]$. (5) If removal is selected and there is not at least one of each type of kink, then abort. Otherwise select kinks of type l_1, l_2, and l_3 for removal with equal probability $1/N_{l_1}$, $1/N_{l_2}$, and $1/N_{l_3}$, respectively.

If configuration $[D]$ has three more kinks than configuration $[C]$, then insertion takes place with probability

$$P[C \to D] = \min\left\{ \frac{(t\beta)^3}{N_{l_1}[D] N_{l_2}[D] N_{l_3}[D]} e^{A[C] - A[D]}, 1 \right\} \quad (4)$$
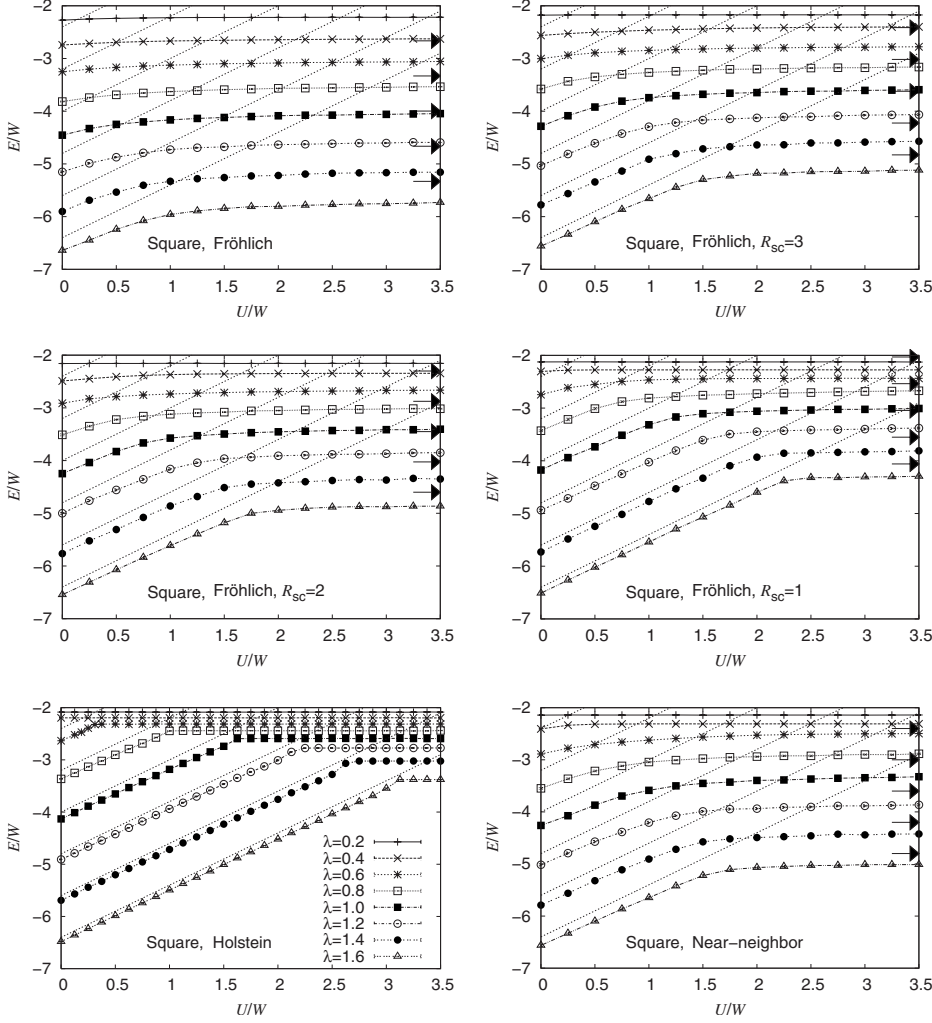
and for removal,

FIG. 1. Total energy of bipolarons on the square lattice for various U, λ, R_{sc}, $\bar{\omega} = 1$ and $\bar{\beta} = \beta/t = 14$. There is a clear qualitative difference between bipolarons with long-range interactions and those formed from the purely local Holstein interaction. Unless otherwise indicated, error bars represent three standard deviations. Where error bars are not visible, they are smaller than the points.

$$P[D \rightarrow C] = \min\left\{\frac{N_{l_1}[D]N_{l_2}[D]N_{l_3}[D]}{(t\beta)^3}e^{A[D]-A[C]}, 1\right\}. \quad (5)$$

Note that the number $N_{l_1}[D]$ represents the number of kinks of type l_1 in configuration D. Therefore when kinks are inserted, this is the number of kinks in the final configuration. When kinks are removed, $N_{l_1}[D]$ is the number of kinks in the initial configuration.

B. Path exchange in 2D

There are some differences between exchange updates in 1D and 2D, and some additional considerations on the triangular lattice. In 1D, exchange can be carried out by inserting and removing kinks and antikinks. The form of the exchange update in 1D is

$$P(C \rightarrow D) = \min\{1, Q_{l,-l}^{(A)}Q_{-l,l}^{(B)} \exp(A[C]-A[D])\}, \quad (6)$$

where

$$Q_{l,-l}^{(A)} = (t\beta)^{2n_A-\Delta}\frac{\min(N_{A-l},\Delta)+1}{\min(N_{Al}+n_A,\Delta)+1}\frac{_{N_{A-l}}P_{\Delta-n_A}}{_{N_{Al}+n_A}P_{n_A}}, \quad (7)$$

here Δ is the displacement between the $\tau = \beta$ ends of path A and path B. $_{n}P_{k} = n!/(n-k)!$ is the number of permutations. There are $N_p = \min(N_{A-l},\Delta)+1$ possible updates that can be made by inserting n_A kinks into path A and removing m_A antikinks, where $n_A + m_A = \Delta$. m_A is chosen with equal weighting $1/N_p$. N_{Al} is the number of kinks of type l on path A. The expression for path B is similar but the kink and antikink assignments are reversed to get displacement $-\Delta$.

In 2D, two sets of kinks and antikinks in different directions are required to exchange the ends of the paths, so the exchange update has the form

$$P(C \rightarrow D) = \min\left\{1, \exp(A[C]-A[D])\prod_{i=1}^{d}Q_{l_i,-l_i}^{(A)}Q_{-l_i,l_i}^{(B)}\right\}, \quad (8)$$

where there is a different Δ for each kink type to be inserted (and thus a different N_p and m which should be chosen independently for each kink type and path) as determined from the number of kinks that would be required to hop from the
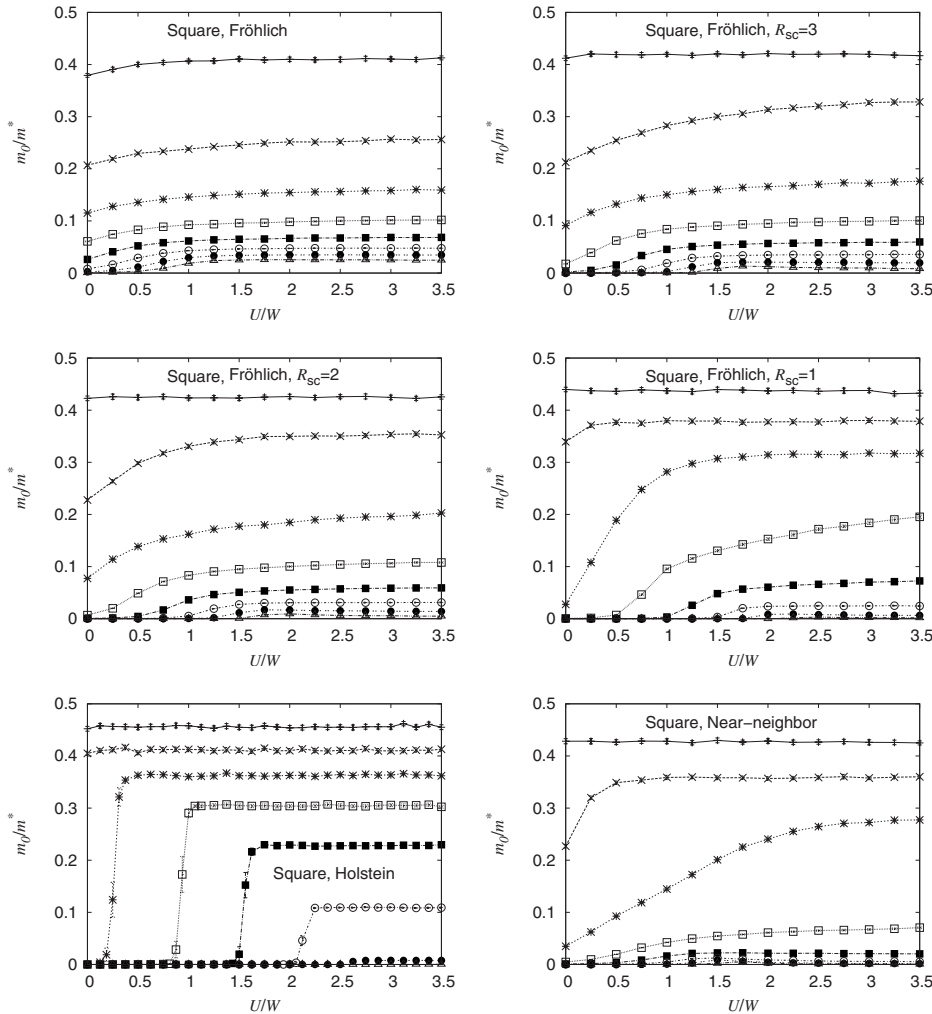
FIG. 2. Inverse mass of bipolarons on the square lattice. Parameters are the same as in Fig. 1. Again, qualitative differences between the bipolarons formed via the purely site local Holstein interaction and the long-range interactions can be seen.

end of one path to the end of the other. d is the number of lattice dimensions.

For the triangular lattice, the choice of the two kink directions is not unique since the kinks are not orthogonal. There are six nearest-neighbor vectors representing kinks. To carry out the update, kinks representing two different directions are chosen with equal weight from all available possibilities (that is, the two chosen kinks may not be antikinks of each other). Since an equal weight scheme is used, the factors relating to the probability of this choice cancel on both sides of the balance equations. It is important to choose kinks from all possible directions to improve the efficiency of the algorithm.

C. Global path shifts

As in the 1D case, a useful update displaces a single path when the configurations are not exchanged. In both cases, one of the paths is chosen with equal probability, a kink direction is chosen with equal probability and then the path is shifted through r lattice sites, where r is an integer chosen randomly between 0 and $R_{\max} - 1$. Typically $R_{\max} = 50$ for lattice size 100. Failure to include global path shifts leads to an inefficient algorithm with large correlation between measurements, which is especially bad when the bipolaron is only

just bound. Global shifts are essential when the bipolaron radius is to be measured.

D. Signs and triplet states

We have previously discussed triplet formation in 1D.[6] When triplets properties are calculated, there is a potential sign problem: for paths in an exchanged state, triplet states pick up a sign $s = -1$, and when both paths begin and end on the same site, a sign $s = 0$ is assigned. In 1D, it is possible to compute triplet properties with configurations that always have sign 1 by selecting $U = \infty$ because triplet properties are independent of Hubbard U (there is a node in the wave function for zero particle separation, so the U has no effect on the triplet state). In 2D, even the $U = \infty$ state has an average sign which is not unity because paths can twist around each other to give an exchanged state even when $U = \infty$. In our calculations of triplet properties we therefore take account of the triplet sign in our averages as discussed in Ref. 6. So long as U is taken to be sufficiently large, the sign problem is not pronounced enough to stop us from computing accurate triplet properties on 2D lattices, although it is necessary to take significantly more Monte Carlo steps to get accurate data.

E. Error estimation

To ensure that errors are estimated with good accuracy, blocking in association with bootstrap resampling is used to
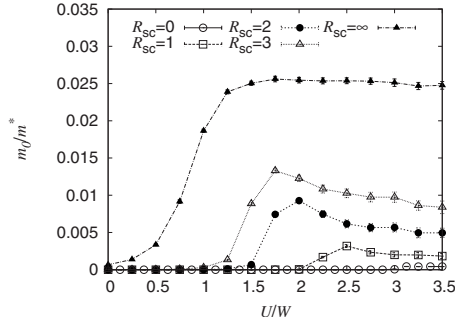
FIG. 3. Comparison of the inverse mass for bipolarons on the square lattice. $\lambda = 1.6$ and various interaction ranges are considered. Other parameters are as in Fig. 1. At intermediate U, the energies of the on-site (S0) and intersite (S1) bipolarons are degenerate, so a light bipolaron can be formed without the need for triangular plaquettes.

avoid underestimating the error because of intertime-step correlations. Where ratios of measurements are considered, the covariance between the two measurements is also taken into account.

III. SINGLETS ON THE SQUARE LATTICE

The survey of the bipolaron parameter space begins by considering singlet properties of bipolarons on the square lattice. We will examine the effects of the electron-phonon coupling, Hubbard repulsion, and interaction range on the bipolarons. In the following, we take $\bar{\omega} = \omega/t = 1$, which corresponds to $\omega/W = 1/4$ which is well inside the adiabatic regime. W is the energy of a single noninteracting electron. $W = 4t$ for the square lattice and $W = 6t$ for the triangular lattice. We restrict paths to lie within 100 lattice spacings of each other, with the large lattice size used to ensure that the effects of the lattice restriction are minimal (this should be true where the bipolaron radius is much smaller than the lattice size). Most properties are not strongly affected by finite-size effects. We note that the inverse radius is the most sensitive measurement, and the total energy the least sensitive. The most severe finite-size effect is that premature binding can occur if the paths are too closely restricted.

Figure 1 shows the total energy of the two polarons/bipolaron pair for a range of electron-phonon coupling strengths, interaction screening radius, and Hubbard U. As is the case in 1D,[6] a qualitative difference can be seen between bipolarons formed with Holstein and screened Fröhlich inter-
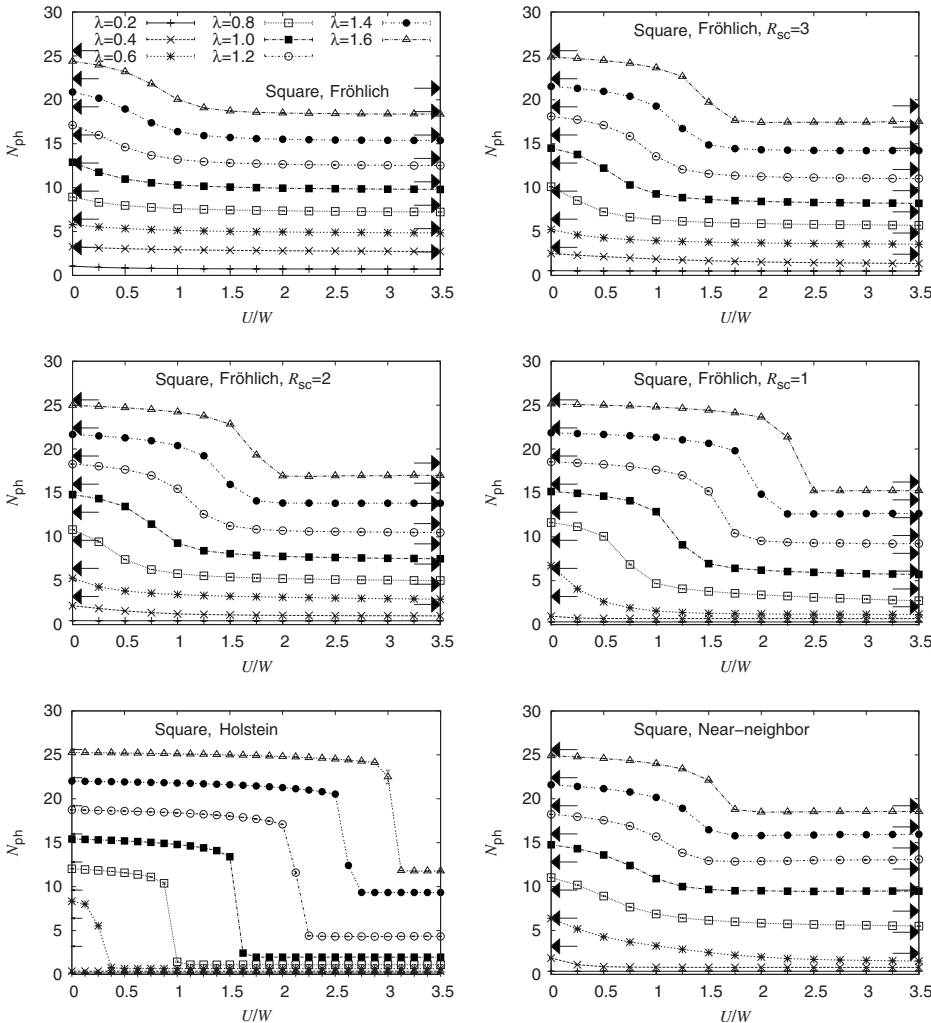

FIG. 4. Number of phonons associated with bipolarons on the square lattice. Parameters are identical to Fig. 1. Again, the properties of the Holstein bipolaron are qualitatively different to those of the Fröhlich bipolaron.
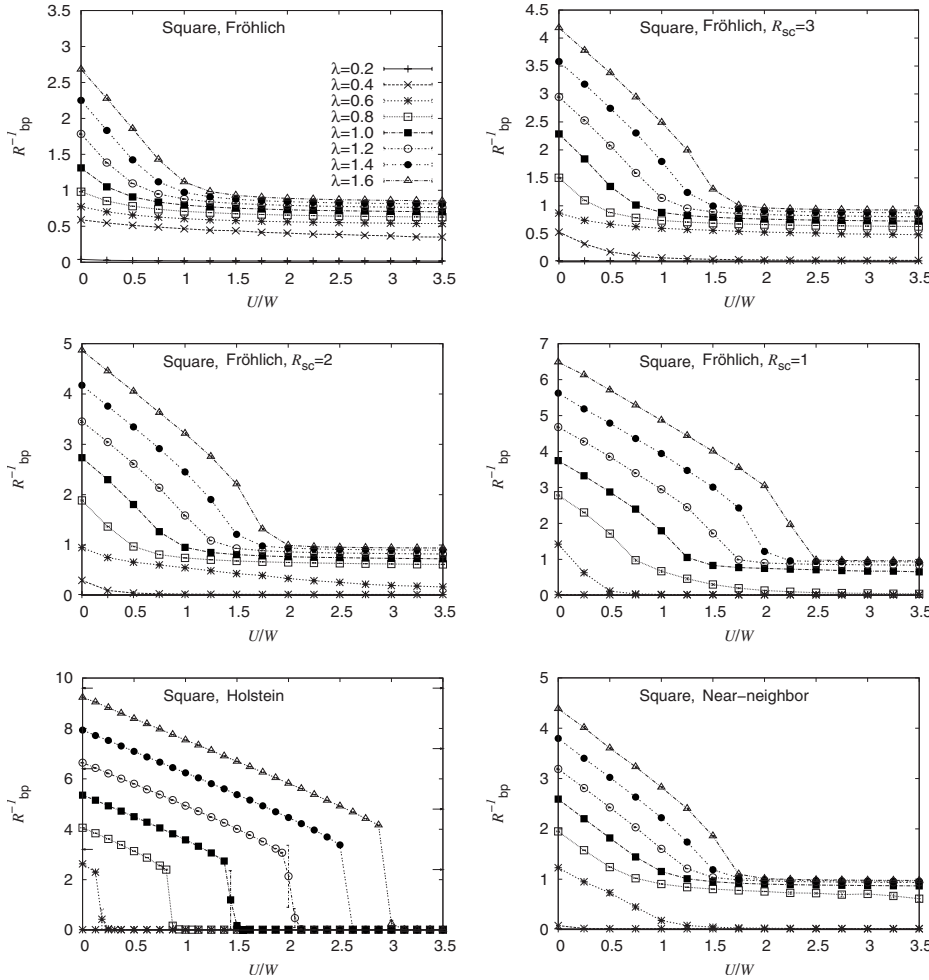
FIG. 5. Inverse bipolaron size associated with bipolarons on the square lattice. Parameters as in Fig. 1.

actions. At large U, the energy curves for the Hubbard-Holstein bipolaron are flat, indicating that the bipolaron has unbound into two polarons. This is true for all the λ shown, indicating that there is no bound singlet bipolaron in the $U \to \infty$ Hubbard-Holstein model. The significance for triplet states will be discussed later in the paper.

In contrast to the flat energy curves characterizing the large U, large λ Holstein model, the energy of the Hubbard-Fröhlich bipolaron changes on varying U, indicating that there are bound singlet states even for very large U (we will revisit this point later in the paper). For small λ and $R_{sc} \neq 0$, the energy curves are flat at large U. The model with only nearest-neighbor interaction $[\Phi(\boldsymbol{a})=0.5]$ has similar properties to the $R_{sc}=2$ and $R_{sc}=3$ models. $\Phi(\boldsymbol{a})=0.438$ to an accuracy of three significant figures for the model with $R_{sc}=2$ and $\Phi(\boldsymbol{a})=0.509$ to an accuracy of three significant figures for the model with $R_{sc}=3$, indicating that bipolaron properties depend most strongly on the nearest-neighbor part of the Fröhlich interaction, rather than the tails.

It is useful to quickly describe the limiting behaviors of the bipolarons. First, it is appropriate to introduce some notation. We use S0 to define a strongly bound on-site singlet pair where the two electrons are separated by no lattice spacings and use S1 to denote a strongly bound intersite pair where the electrons are separated by one lattice space.[14] As discussed for the 1D model,[6] if bipolarons are strongly bound the renormalized intersite hopping is small, and an

atomic Hamiltonian can be determined using the Lang-Firsov transformation,

$$\widetilde{H}_{\mathrm{at}} = -\sum_{\boldsymbol{nn'}} \frac{W\lambda\Phi_0(\boldsymbol{n},\boldsymbol{n'})}{\Phi_0(0,0)}\hat{n}_{\boldsymbol{n}}\hat{n}_{\boldsymbol{n'}} + \omega\sum_{\boldsymbol{m}}\left(d_{\boldsymbol{m}}^{\dagger}d_{\boldsymbol{m}} + \frac{1}{2}\right). \quad (9)$$

Since the electron number operator, $\hat{n}$ is unchanged under the Lang-Firsov transformation, the effects of the Hubbard U can quickly be reintroduced. Thus, for a strongly bound on-site (S0) bipolaron,

$$E = U - 4W\lambda. \quad (10)$$

W is the noninteracting kinetic energy of a single particle (half bandwidth). The limiting behavior of the S0 bipolaron is shown on the plots as dashed lines. As in the 1D case, the S0 Hubbard-Holstein bipolaron rapidly becomes strongly bound on decreasing U. For the longer range interactions, it takes much more attraction to strongly bind the S0 bipolaron. We can also compute the energy of the strongly bound S1 bipolaron which forms at large λ and $U \gg W\lambda$,

$$E = -2W\lambda[1 + \Phi(\boldsymbol{a})/\Phi_0]. \quad (11)$$

The energy of the strongly bound S1 state is plotted in Fig. 1 as the arrows at $U/W=3.5$ (note that only five arrows corresponding to the largest λ are shown). The energy of the strongly bound S1 bipolaron is higher than the simulated energy but the values converge as λ increases. From the
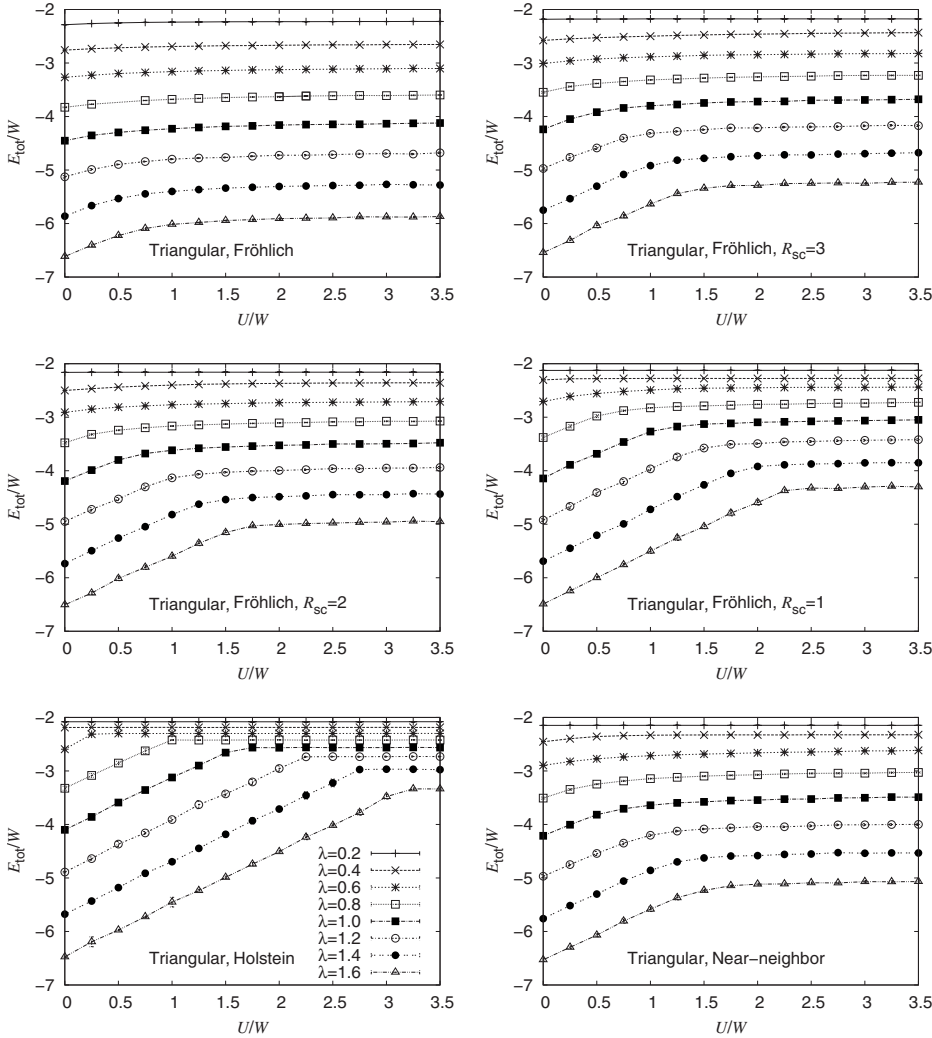
FIG. 6. Total energy of singlet bipolarons on the triangular lattice. $\omega/t=1.5$, U, λ, and R_{sc} are varied, $\bar{\beta}=28/3$. The value of ω/t is chosen so that ω/W is the same for both square and triangular lattices. The energies are qualitatively similar to those associated with the square lattice.

difference in energies between the S1 limit and the simulated energy, it appears that the bipolarons formed from heavily screened interactions have a stronger S1 character.

The inverse mass of the bipolarons is shown in Fig. 2. Again, significant differences between Hubbard-Holstein and Hubbard-Fröhlich bipolarons can immediately be seen. In the Hubbard-Holstein model, the mass changes very rapidly with U when the bipolaron binds, with the mass changing through several orders of magnitude over a very small range of U values. This rapid change is not seen for the Fröhlich bipolaron, which maintains a similar mass over a wide range of U. For the larger λ values and large U, the system of two particles appears to be heavier in the Fröhlich case. This is because the Holstein bipolaron is not bound for those values, whereas the Fröhlich interaction leads to an intersite (S1) bipolaron.

In comparison to the U dependence of the mass of the 1D Holstein bipolaron, which can be found in Ref. 6, the change in mass with U is extremely rapid on the square lattice. In contrast, the mass relating to long-range interactions is qualitatively unchanged, with the formation of a relatively light bipolaron (even in comparison with a free electron) over a very wide range of the parameter space. The qualitative difference between the properties of Holstein and Fröhlich bipolarons emphasizes that while the Holstein model may be a

reasonable approximation for considering polarons in organic molecular compounds, the simple Holstein approximation is inappropriate for many crystalline systems where complete screening of the electron-phonon interaction is not possible. Even if the screening length is as small as a single lattice spacing, bipolarons have significantly modified properties compared with those formed in the Holstein model.

In 1D, a crablike bipolaron can form in models with long-range interaction when the energies of on-site and off-site configurations are degenerate (S1 like configurations can be changed to S0 with a single hop, without any energy barrier to make the process second order in t). This leads to a noticeable decrease in mass at intermediate U. It is of interest to determine if these lighter bipolarons can also form on the square lattice. In Fig. 3, the masses of bipolarons formed when $\lambda=1.6$ are examined as R_{sc} is changed. A peak in the inverse mass (decrease in the mass) is clearly visible at intermediate U and is especially pronounced when $R_{sc}=2$. Comparing Eqs. (10) and (11), it can be seen that for large phonon frequencies, the peak would be expected at $U/W = 2\lambda[1-\Phi(\boldsymbol{a})/\Phi(0)]$, which corresponds to $U/W=1.798$ for $R_{sc}=2$ (to 4 significant figures) in good agreement. The presence of this peak shows that light bipolarons can exist on square lattices without the need for triangular plaquettes. Naturally, such a state depends on a very subtle balance of
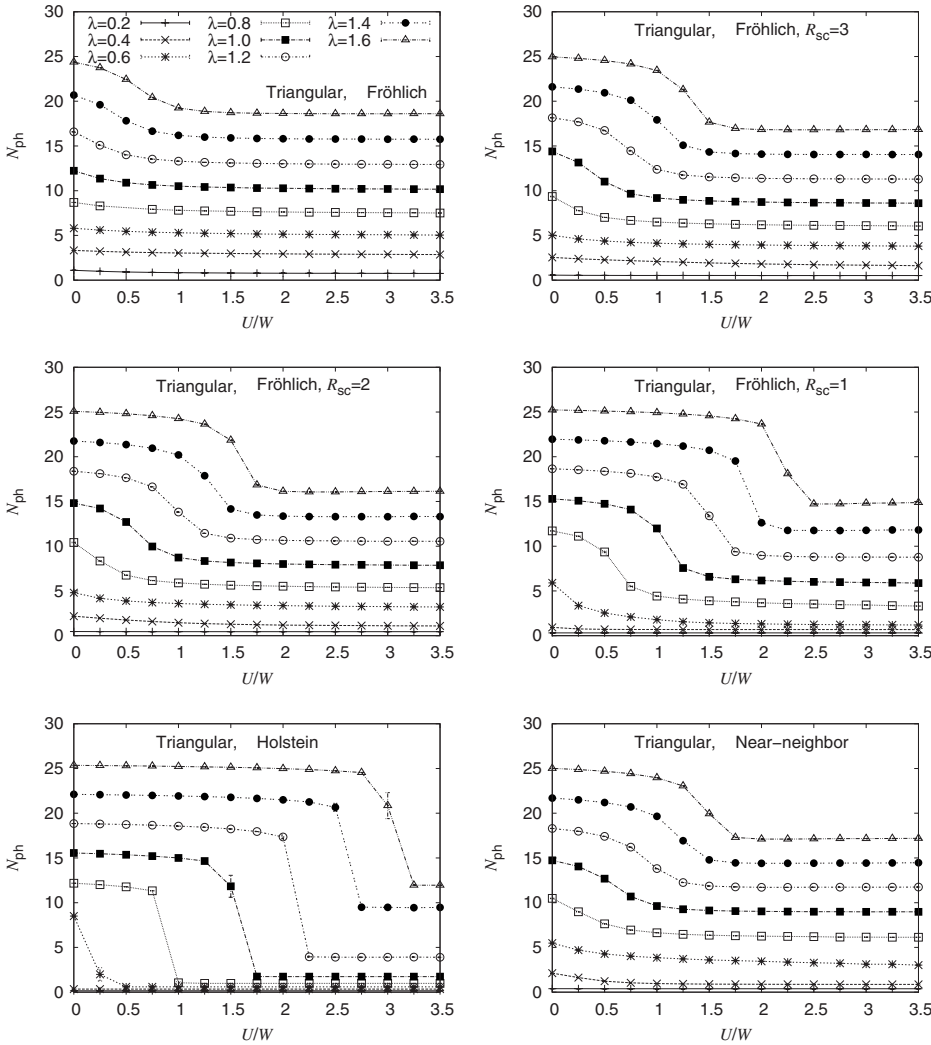
FIG. 7. Number of phonons associated with bipolarons on the triangular lattice. Parameters are as in Fig. 6.

parameters and could not be realized in all crystalline systems.

As in the case of the 1D bipolaron, analytical determination of the effective mass, even for limiting values of the parameters, is difficult (and may not be possible) when there are long-range tails in the interaction. While we have not computed limiting behaviors of the mass for the model with only near-neighbor interaction, we expect that a similar approach to that applied to the 1D bipolaron by Bonča and Trugman[21] could yield results.

We also show the number of phonons associated with the bipolaron cloud (Fig. 4). As before, the properties of the Hubbard-Holstein bipolaron are qualitatively different to the bipolarons formed from long-range electron-phonon interaction. The number of phonons associated with the Holstein bipolaron shows an abrupt increase as the bipolaron binds on decreasing U, whereas there is a smoother crossover from S1 to S0 behavior associated with the screened Fröhlich interaction.

The total number of phonons associated with the strongly bound on-site bipolaron (following the argument in Ref. 12) is

$$N_{\mathrm{ph}} = \frac{4W\lambda}{\omega}. \qquad (12)$$

This number is independent of U, so the number of phonons reaches a limiting value on decreasing U as seen in Fig. 4 (the strongly bound S0 limit is represented by arrows on the left of the graph). The Holstein bipolaron with large λ quickly reaches the S0 limit at low U. Bipolarons formed with long-range interactions approach the S0 limit less rapidly since the longer range tails lead to a shallower effective potential.

The number of phonons associated with the S1 bipolaron can also be found,

$$N_{\mathrm{ph}} = \frac{2W\lambda}{\omega}\left[1 + \frac{\Phi(\boldsymbol{a})}{\Phi_0}\right]. \qquad (13)$$

This is represented as arrows on the large U side of the plots. The agreement improves on increasing λ. Again, it is clear that the most heavily screened interactions have the most clearly defined S1 character.
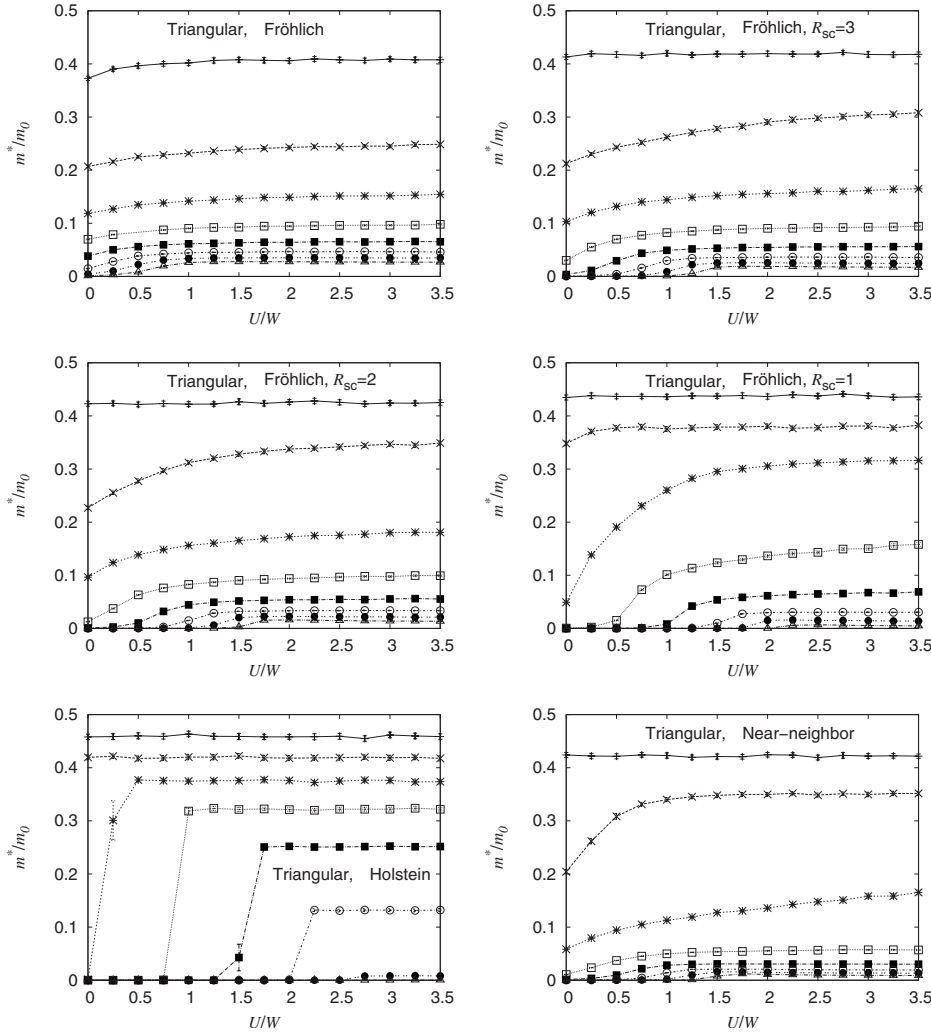
FIG. 8. Inverse mass of bipolarons on the triangular lattice. Parameters are as in Fig. 6. The mass decrease at intermediate U is much smaller than in the case of the square lattice since the intersite bipolarons formed at large U/t are already superlight.

We complete this section by examining the inverse bipolaron size associated with the square lattice (Fig. 5). Again, qualitative differences exist between the Holstein bipolaron and the Fröhlich bipolarons, with S1 bipolarons forming in the screened Fröhlich model at large U and λ indicated by a radius of around a lattice spacing. Comparison with Fig. 2 shows that bipolarons on the square lattice with long-range interaction may be both small and light at intermediate and large λ and intermediate U, where polarons are bound into the hybrid S0-S1 bipolaron.

IV. SINGLETS ON THE TRIANGULAR LATTICE

In this section, attention is turned to the properties of bipolarons on the triangular lattice, which have already been shown to have unusual properties.[12] To ensure that results for bipolarons on square and triangular lattices can be meaningfully compared, we have kept energy scales fixed in terms of W (the noninteracting kinetic energy of a single particle) rather than t. For the square lattice, $W=4t$, while for the triangular lattice, $W=6t$. Similar considerations should be made when comparing plots of total energy between lattice types, which is why we have quoted all energy scales in these sections in terms of W. Also, to keep the ratio $\omega/W=1/4$, all properties in this section are computed for $\omega/t=1.5$. Finally, for the same reason, the temperature is also $3/2$ higher than that used for computations of the bipolaron on the square lattice, so $\bar{\beta}=28/3$.

Figure 6 shows the total energy of bipolarons on the triangular lattice as U, λ, and R_{sc} are changed. A quick inspection indicates that there is no clear qualitative difference between the total energy of bipolarons on square and triangular lattices. The same is true of the number of phonons associated with the bipolaron, which is shown in Fig. 7. It is quite
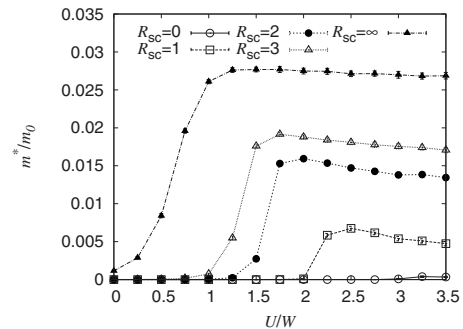

FIG. 9. Comparison of the inverse mass at $\lambda=1.6$ for bipolarons on the triangular lattice. Parameters are as in Fig. 6.
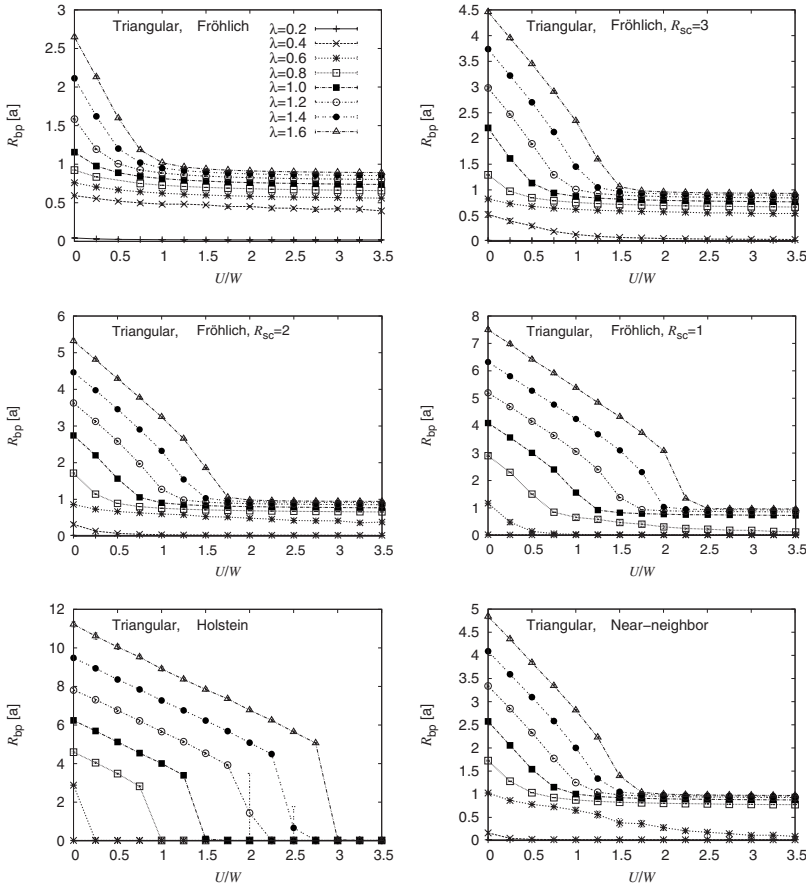
FIG. 10. Inverse size associated with bipolarons on the triangular lattice. Parameters are as in Fig. 6.

surprising that the properties are so similar since there are very different hopping mechanisms on the triangular lattice compared to the square lattice (such as the possibility for S1 bipolarons to move with a single hop on the triangular lattice while intersite bipolarons on the square lattice have to tunnel through a high-energy intermediate state to move). However, careful comparison shows that in the strong U limit (where intersite S1 bipolarons are formed) the bipolaron formed from near-neighbor interactions has slightly more phonons on the square lattice than on the triangular lattice. For the very long-range Fröhlich interaction, there are only tiny differences between results for the square and triangular lattices (there are around 2.5% more phonons associated with

Fröhlich bipolarons on the triangular lattice). Clearly, the crossover between S0 and S1 bipolarons occurs at approximately the same value of U/W. The strong similarities between the properties of bipolarons on square and triangular lattices on the adiabatic side of the parameter space is quite surprising considering that the properties are very different in the antiadiabatic limit. However, the differences between the bipolarons become clearer when the inverse mass is examined.

It has previously been reported that bipolarons on the triangular lattice are small and light.[12] Figure 8 shows the inverse mass of bipolarons on the triangular lattice. Bipolarons formed via the Fröhlich interaction are relatively light, as
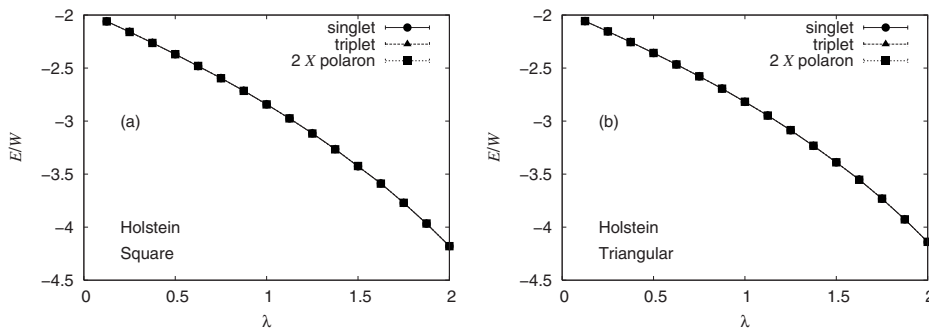

FIG. 11. Absence of triplet bipolaron in the Holstein model on square and triangular lattices. (a) Square lattice, $\bar{\beta}=7$, $\bar{\omega}=1$, and $U/t=40$. (b) Triangular lattice, $\bar{\beta}=14/3$, $\bar{\omega}=1.5$, and $U/t=60$. Properties are computed at various λ. Note that with the energy expressed in terms of the bandwidth, lattice type has very little effect on Holstein polarons. The singlet and triplet curves lie under the polaron curve and are identical to within the statistical error.
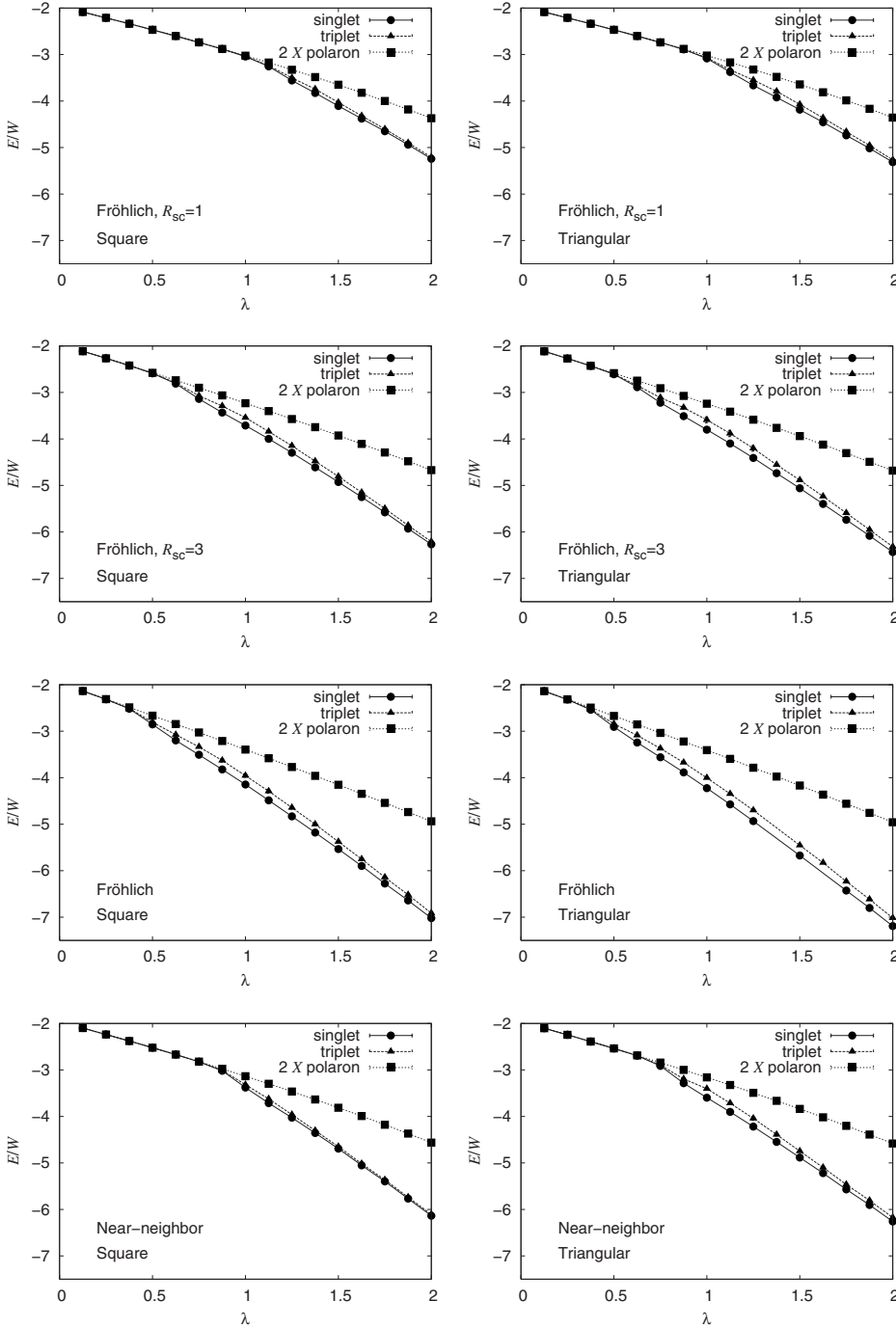
FIG. 12. Total triplet energy of the Fröhlich bipolaron on the square lattice (left) and triangular lattice (right). For the square lattice, $U=40t$, $\bar{\beta}=7$, and $\bar{\omega}=2$. On the triangular lattice, $U/t=60$, $\bar{\omega}=3$, and $\bar{\beta}=14/3$. λ and the interaction range are varied. For comparison, we also show the singlet energy and the energy of two polarons. As the interaction range increases, the minimum electron-phonon coupling required to bind both singlet and triplet decreases. The singlet energy is very similar on both lattices. However, the singlet-triplet splitting on the triangular lattice is much larger than on the square lattice for all interaction ranges.

was observed when the square lattice was considered. The Holstein bipolaron remains qualitatively different to the bipolarons formed with the screened Fröhlich interaction, with an enormous change in the mass of several orders of magnitude over a very small range of U/W as the bipolaron binds. The most significant (and surprising) differences between the bipolarons on square and triangular lattices can be seen when nearest-neighbor interactions are considered and when $\lambda=0.6$ and U is large. For these parameters, the bipolaron on the square lattice is lighter than its counterpart on the triangular lattice (although this does not mean that it is necessarily small). We also note that as λ approaches 1.6, the relative magnitudes of the masses on square and triangular lattices

reverses and the bipolaron on the triangular lattice becomes lighter than the bipolaron on the square lattice (the other parameters are held fixed). This is the part of the parameter space where superlight small bipolarons are expected. We will revisit this point when the size of the bipolaron is computed.

Again, a hybrid S0-S1 bipolaron is likely when the S0 and S1 configurations become degenerate. As before, this state is visible as a decrease in the effective mass (increase in inverse effective mass) at intermediate U. A comparison of the inverse masses of bipolarons as interaction range is changed is shown in Fig. 9. There is only a shallow maximum in the inverse mass curve for $R_{sc}=\infty$ but there are more pronounced
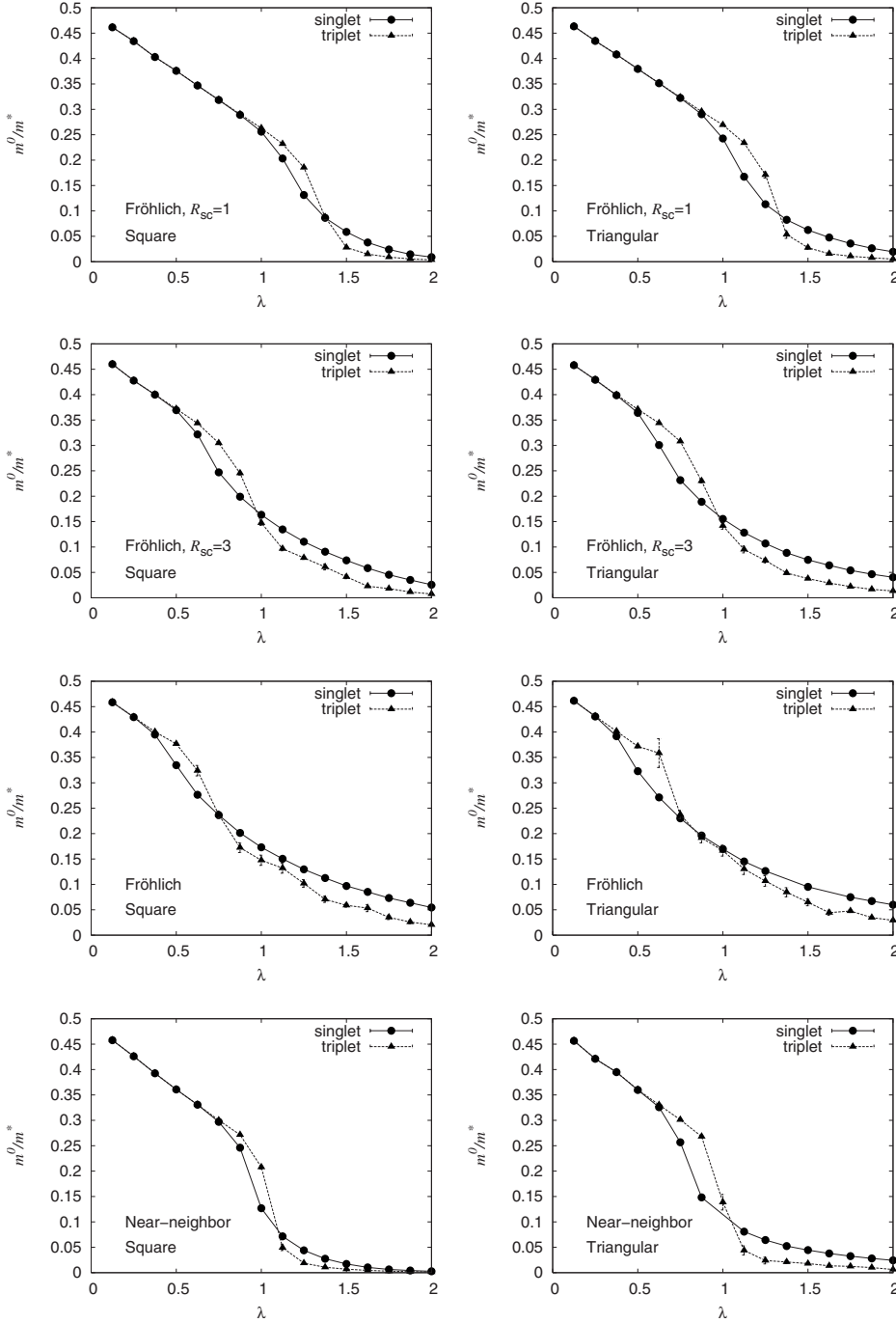
FIG. 13. Inverse mass of the triplet Fröhlich bipolaron. Parameters are as Fig. 12. Error bars represent one standard deviation. At low λ, the triplet bipolaron is lighter than the singlet bipolaron. Note that since properties of the triplet bipolaron do not depend on U, then the singlet will be always be heavier at low U.

humps in the curves for smaller values of the screening, corresponding to a light bipolaron. The peaks are not as pronounced for the bipolaron on the triangular lattice as they were when motion was on the square lattice. This is probably because the S1 bipolaron on the triangular lattice at large λ and large U is already light and small with a mass that is first order in t,[12] so the presence of the hybrid state does not make it significantly easier for the bipolaron to move about on the triangular lattice (whereas on the square lattice, the change from S1 to the hybrid state changes bipolaron hopping processes from second to first order in t leading to a reduction in mass).

To finish the examination of the differences between square and triangular lattices, we examine the inverse bipo-

laron size in Fig. 10. For large λ, the size of the pair is small and S1 bipolarons are clearly formed in the Fröhlich model at large U (i.e., the radius is approximately one lattice spacing). There are differences between the sizes of bipolarons on triangular and square lattices. Comparison between the radius of the bipolaron on the two lattices shows that the bipolaron on the triangular lattice is significantly smaller than its counterpart on the square lattice at large U. Also, the bipolaron on the triangular lattice is slightly bigger than the pair on the square lattice at very small U. The bipolarons formed on square and triangular lattices have similar size at intermediate U where the pair has hybrid S0-S1 properties. Thus we can see that the slightly larger (but still light) mass of the S1 bipolaron on the triangular lattice is most likely a
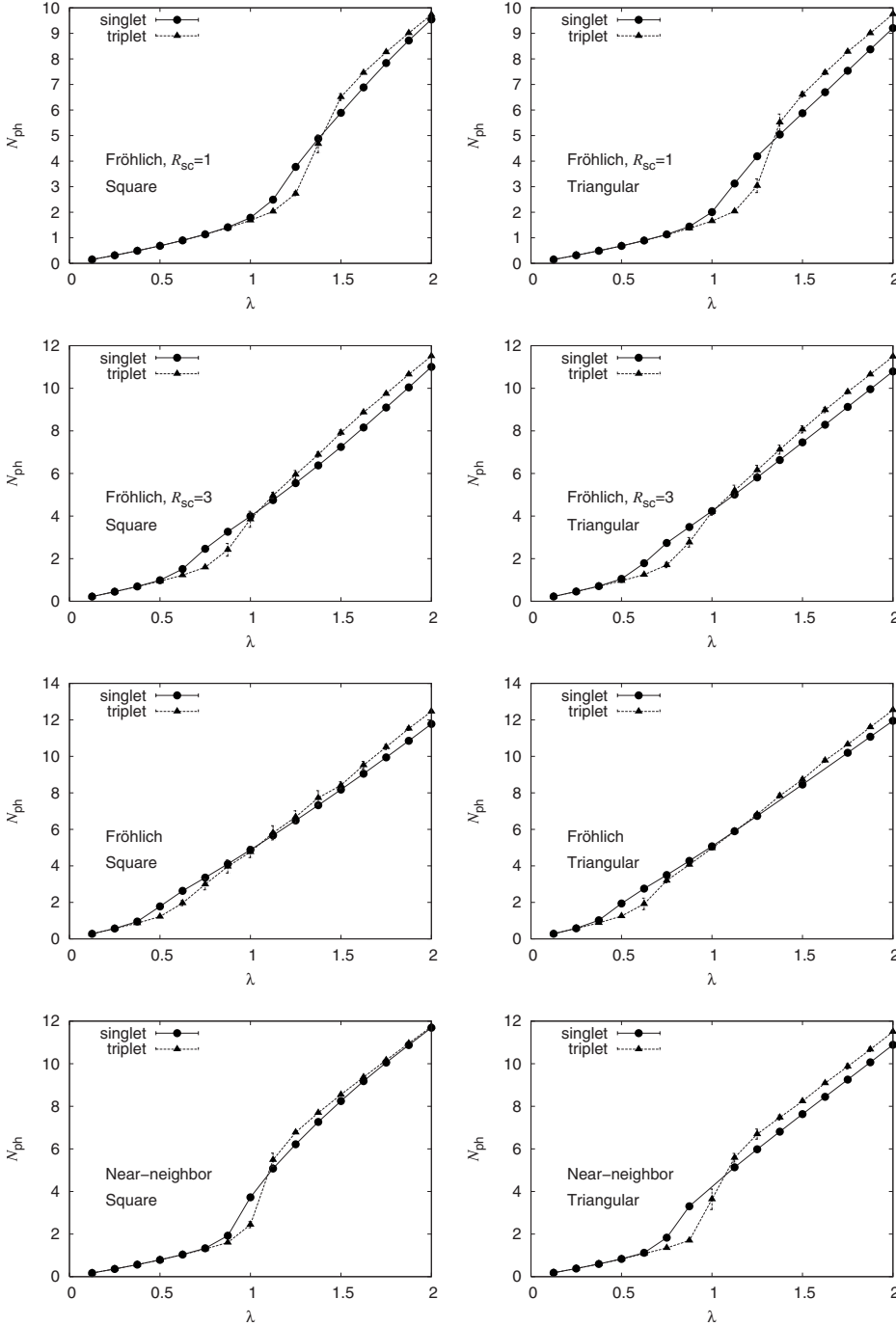
FIG. 14. Number of phonons associated with the triplet Fröhlich bipolaron. Parameters are as Fig. 12.

result of the stronger binding into the S1 state (indeed for large U, the S1 state is very well bound on the triangular lattice at quite small λ—shown by $R_{bp}^{-1} \approx 1$). It is this property of small and light bipolarons that could lead to a bipolaron condensate of S1 bipolarons on a triangular lattice at reasonably high temperatures. However, we have now identified an additional bipolaron configuration which is light and small on both triangular and square lattices, and which is formed at moderate λ and U: the extra-light hybrid S0-S1 bipolaron.

V. TRIPLETS

We now direct our attention to triplet properties of the bipolaron. The possibility of triplet superconductivity has received a lot of interest since the discovery of spin triplet superconductivity in Sr_2RuO_4.[22] Triplet superconductivity has also been identified in heavy fermion materials that have a triangular lattice.[23] From the theoretical point of view, triplet pairs could be of interest for two reasons. First, there is a wide literature on BCS to BEC crossover[24–26] which is of interest when the parameters governing pairing are intermediate. The presence of stable real-space triplet pairs would add additional limits to this problem, including a crossover or transition between singlet and triplet pairings. Second, the energy difference between singlet and triplet states could be considered as the energy cost of a spin flip, with a direct interpretation as a spin gap.[1] In the next two sections of this
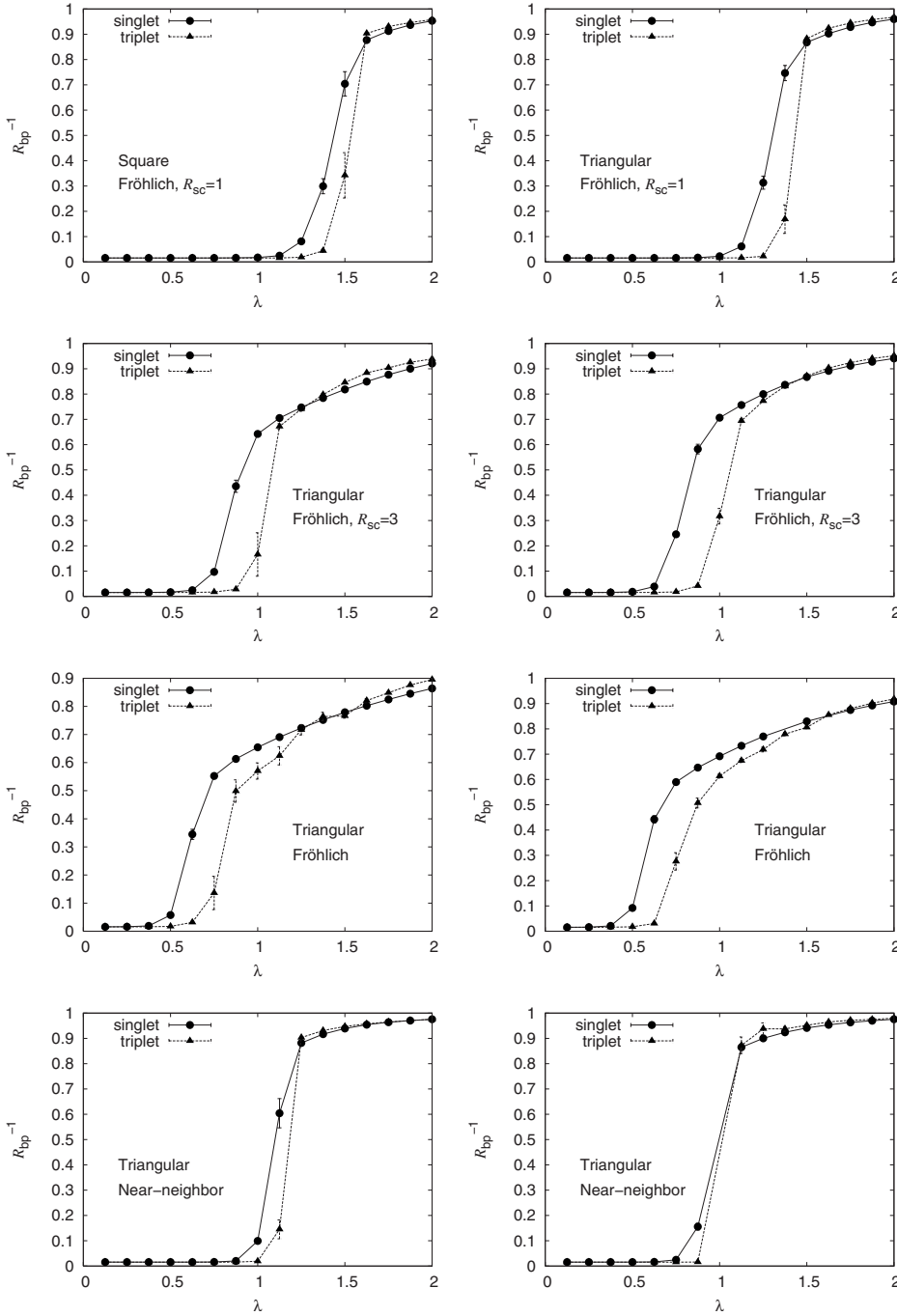
FIG. 15. Radius of the Fröhlich triplet bipolaron. Parameters are as Fig. 12.

paper, we discuss the possibility and properties of real-space triplet pairs on square and triangular lattices.

A. Hubbard-Holstein model

We start our examination by considering the on-site Hubbard-Holstein interaction. To examine if triplet bipolarons can exist in the 2D Hubbard-Holstein model, we examine the model with very large $U/W=10$ and compare the energy of two electrons subjected to the Hubbard-Holstein interaction with that of two unbound polarons (Fig. 11). There are several good reasons for doing this. First, as we have seen in the previous sections, the energy of the singlet bipolaron increases monotonically with U, so the binding energy of the singlet bipolaron is minimized, therefore the singlet triplet splitting is also minimized (since triplet states cannot have a higher energy than two free polarons without dissociating). Second, since triplet states must have equal or higher energy than singlets, an unbound singlet also implies that the triplet is also not bound. The triplet properties cannot depend on U since a node in the triplet pair wave function means that the Hubbard U has no possible effect on triplet properties, so it is sufficient to analyze only this large U limit. We have carefully computed the energies of singlets, triplets, and two polarons on triangular and square lattices, and have found no bound triplet states to within the statistical error.
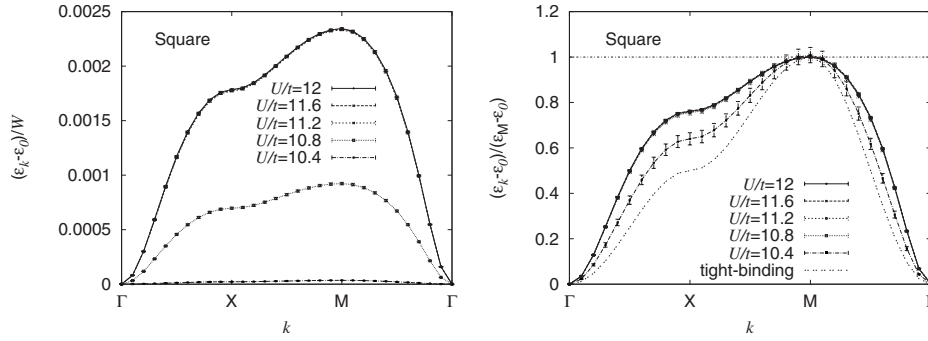
FIG. 16. Singlet dispersions of the Hubbard-Holstein bipolaron on the square lattice when $\lambda=1.45$, $\bar{\beta}=14$, and $\bar{\omega}=1$. U is varied. Note that error bars on the plots of dispersions represent one standard deviation. The lower panel shows the dispersions normalized by $\epsilon_M-\epsilon_0$ compared to the normalized tight-binding dispersion. As U decreases, the bipolaron becomes strongly bound on-site and the dispersion develops a form closer to the tight-binding approximation.

B. Hubbard-Fröhlich model

While there are no triplet bipolarons formed in the Hubbard-Holstein model, the longer range interactions associated with the Hubbard-Fröhlich model can lead directly to intersite pairing, which is likely to lead to triplet states. To determine the existence of triplet pairs in the model, we compute the singlet and triplet energies, and compare them with the energy of two polarons, which can be seen in Fig. 12. The parameters associated with the computations are $U=40t$, $\bar{\beta}=7$, and $\bar{\omega}=2$ on the square lattice and $U/t=60$, $\bar{\omega}=3$, and $\bar{\beta}=14/3$ on the triangular lattice. We use the same parameters throughout this section. At weak λ, there are neither singlet nor triplet bound states. On increasing λ, the singlet and triplet states bind at a similar value of λ (the binding can be seen as bifurcations of the curves). At very large λ, the energies of the singlet and triplet become degenerate. This is a result of the interaction on the polaron hopping, which becomes exponentially small. The separation of singlets and triplets in the U-V model on the square lattice scales as t^2, whereas on the triangular lattice the large λ singlet-triplet splitting scales like t. This can be seen in the adiabatic limit as a much larger singlet triplet splitting in the case of the triangular lattice. We note that there are strictly two degenerate triplet states measured here, representing two p pairings.

The inverse mass of the triplet Fröhlich bipolaron is shown in Fig. 13. At this value of U/W and large electron-phonon coupling, the triplet bipolaron is heavier than the singlet bipolaron, and at weak coupling the triplet is lighter. As U is changed, the triplet properties remain constant, whereas the singlet ones change, notably with an increase in the singlet mass on decrease in U. At very small U, we would expect that the singlet is always heavier. While the strongly coupled singlet bipolaron is clearly lighter on the triangular lattice, which is due to the qualitative effects of lattice type, we do not see any qualitative difference between the mass of the triplets on square and triangular lattices which are very similar.

Figure 14 shows the number of phonons associated with the triplet Fröhlich bipolaron. At strong coupling on the triangular lattice, there is a clear difference between the number of phonons associated with singlet and triplet. In contrast, on the square lattice the number of phonons associated with the two types of bipolaron converges on a single value at large λ. We believe that this is related to the second-order hopping on square lattices at strong coupling and first-order hopping on triangular lattices. We also note that increasing the electron-phonon interaction range reduces this difference, presumably since the bipolaron has more configurational freedom when R_{sc} is increased, thus allowing similar hopping processes.

Finally, we compute the radius of the triplet Fröhlich bipolaron, which is shown in Fig. 15. There are only small quantitative changes between the radii of triplet bipolarons on different lattices. We note a small finite-size effect at weak coupling, which corresponds to a finite inverse radius where the bipolaron is not bound. On increasing λ, the singlet bipolaron is the first to bind strongly, with the triplet radius decreasing slightly but with the triplet becoming small only for larger λ. Increased interaction range decreases the electron-phonon coupling required to bind both types of bipolaron. The strongly bound triplet is slightly larger than the singlet.

VI. DISPERSION

A. Hubbard-Holstein model

To complete our survey of bipolarons in 2D, we consider dispersions of the Hubbard-Holstein and Hubbard-Fröhlich bipolarons. The electron-phonon interaction has the potential to lead to unusual effects. For example, polaron dispersions in the adiabatic regime of the Holstein model on square and triangular lattices are flattened at the edge of the Brillouin zone.[27,28] It is not known if the dispersion remains flattened once bipolarons form, and also little is known about the dispersions of triplet bipolarons. Thus, it is of interest to determine how the flat dispersion evolves as a bipolaron is bound from two polarons.

In Fig. 16 we show singlet dispersions of the Hubbard-Holstein bipolaron on the square lattice when $\lambda=1.45$ and $\bar{\omega}=1$. Computation of the dispersion is carried out using the same method as in Ref. 6. At large U, the bipolaron is unbound and the dispersion represents two polarons.[29] The dis-
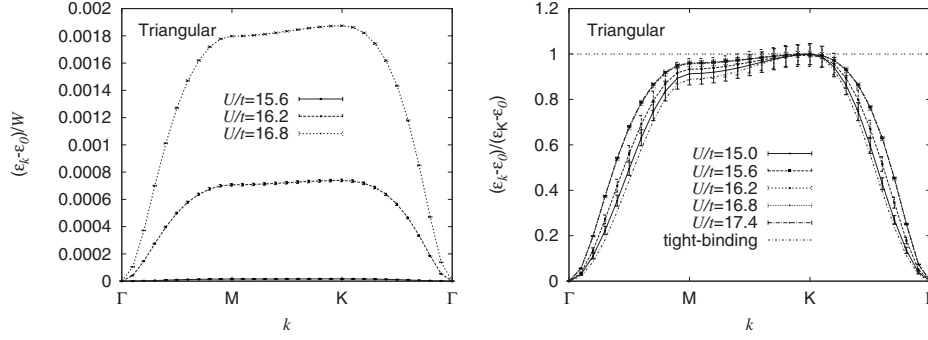
FIG. 17. Singlet dispersions of the Hubbard-Holstein bipolaron on the triangular lattice when $\lambda = 1.45$, $\bar{\beta} = 28/3$, and $\bar{\omega} = 1.5$. U is varied. Error bars represent one standard error. There is a very rapid change in the bandwidth between $U/t = 15.6$ and $U/t = 16.8$. This coincides with a change in the shape of the dispersion from the flattened to the tight-binding form.

persions relating to $U/t = 12$, $U/t = 11.6$, and $U/t = 11.2$ are indistinguishable to the eye (left panel). As the repulsion is decreased, there is a decrease in bandwidth of several orders of magnitude at the U corresponding to the binding of the bipolaron. In the right panel, we also show dispersions normalized by $\epsilon_M - \epsilon_0$ (ϵ_M is the energy of the bipolaron at the M point) so that the forms of the dispersion function can be compared to the noninteracting tight-binding dispersion. At large U, the form of the dispersion of the two polarons (and the weakly bound bipolaron) is quite distorted away from the form of the tight-binding dispersion. As U decreases further, the electrons become tightly bound into an on-site bipolaron. Then the form of the dispersion tends toward that of the tight-binding spectrum. We believe this to be the effect of the strongly bound bipolaron acting as a single particle, with a new hopping integral that relates to the overlap of the wave function of the pair between sites.

In Fig. 17 we show the variation in the singlet dispersions of the Hubbard-Holstein bipolaron on the triangular lattice when $\lambda = 1.45$, $\bar{\omega} = 1.5$, and U is varied. Again, the functional form of the spectrum tends toward the tight-binding disper-

sion as pairs become strongly bound, although it becomes increasingly difficult to collect data since the fractional variance on the dispersion increases as λ increases. Again, we suggest that the similarity in functional forms is due to the tightly bound bipolaron acting as a single particle with a single (albeit small) intersite hopping parameter. For the Holstein bipolaron, the pair wave function is small and the lattice distortion is highly localized.

B. Hubbard-Fröhlich model

We also examine the dispersions of the Hubbard-Fröhlich model. In Fig. 18, we show the dispersion for the square lattice when the Fröhlich interaction with $R_{sc} = 2$ is considered. The panels show the effects of changing U. At large U, the bipolaron is bound into an intersite (S1) configuration. There are two main features that should be emphasized. The first is remarkable. As the Coulomb repulsion decreases, the bandwidth *increases* significantly, i.e., although the bipolaron becomes more strongly bound, it becomes lighter. This is the same effect as seen in Sec. III, where the mass was
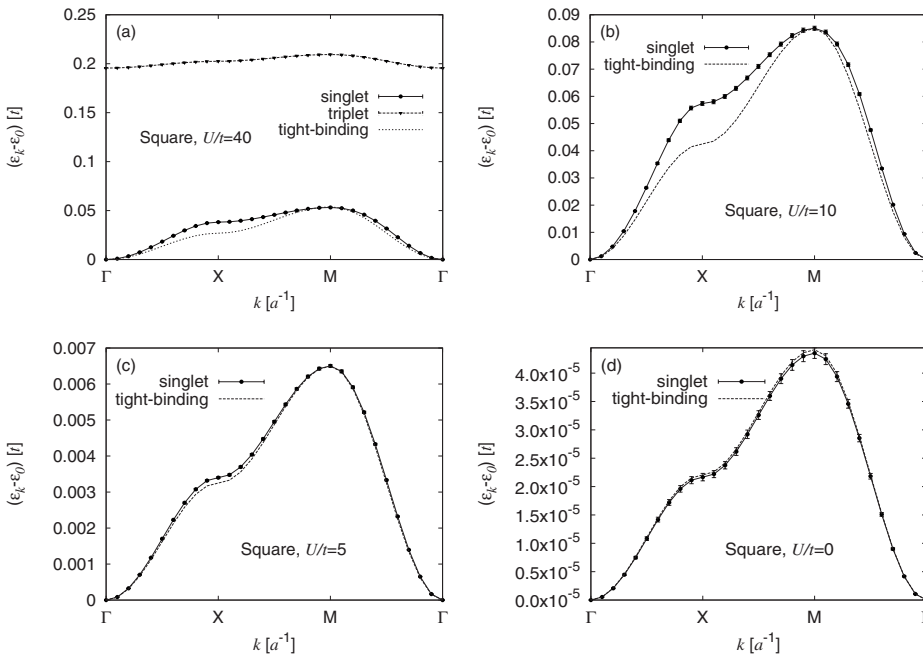

FIG. 18. Singlet dispersions of the Hubbard-Fröhlich model on the square lattice. The triplet dispersion is shown in panel (a). For comparison, the tight-binding dispersion normalized to the bandwidth is also shown. $\lambda = 1.45$, $\bar{\omega} = 1$, $R_{sc} = 2$, and $\bar{\beta} = 14$. Error bars show one standard deviation. As U decreases and the bipolaron becomes strongly bound on-site, the shape of the dispersion becomes consistent with that of a tightly bound particle. An increase in the bandwidth can be seen initially on decreasing U corresponding to the formation of the hybrid S0-S1 bipolaron. For smaller U, the S0 bipolaron is tightly bound and the dispersion is narrow.
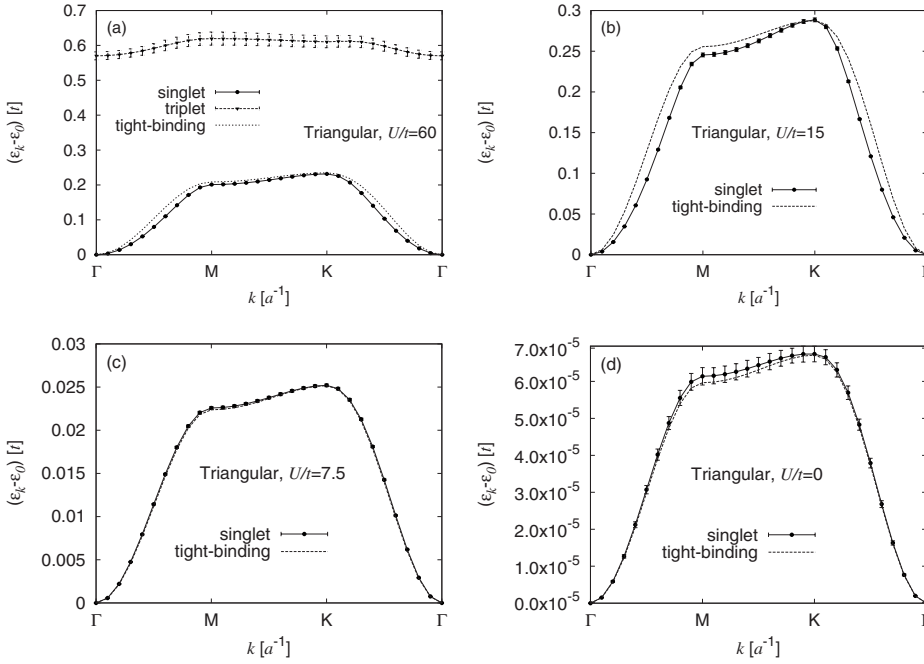
FIG. 19. Singlet dispersions of the bipolaron formed in the screened Hubbard-Fröhlich model on the triangular lattice. $R_{sc}=2$, $\lambda=1.45$, $\bar{\omega}=1.5$, $\bar{\beta}=28/3$, and U is varied. Error bars represent one standard deviation. As U is decreased, the bandwidth initially increases as the S0-S1 hybrid bipolaron is approached from the S1 bipolaron (until around $U/t=15$). For small U, the S0 bipolaron is approached and the bandwidth decreases significantly. For reference the tight-binding dispersion normalized to the same bandwidth is also plotted. The triplet dispersion is shown in panel (a).

shown to decrease at intermediate U as a new type of hybrid S0-S1 crab bipolaron forms. At small U, the degeneracy of the S0 and S1 bipolarons is broken and the bandwidth decreases with U.

The second feature in Fig. 18 is that the shape of the bipolaron dispersion changes dramatically as it is bound on-site. For large U, the dispersion is flattened, whereas for the strongly bound on-site pair ($U/t=5$) the dispersion has the characteristic tight-binding shape (albeit strongly renormalized by interactions). We consider this effect to relate to the change between hopping mechanisms. For a weakly bound bipolaron, the wave function is large and single polaronlike hops dominate the motion of the particle, whereas for the strongly bound bipolaron, the pair wave function is smaller than a single lattice site and a new hopping integral becomes relevant, which is relating to the tunneling of the whole bipolaron between sites. The dispersions of triplet states on the square lattice are also shown in the panel relating to $U/t=40$. The triplet state is higher in energy and has a narrower bandwidth. Singlet and triplet dispersions do not cross.

We also examine the dispersions of the Coulomb-Fröhlich bipolaron on a triangular lattice, which are shown in Fig. 19. The first significant difference between bipolarons on square and triangular lattices is the existence of superlight bipolarons at large $U \rightarrow \infty$. These contribute to a factor of ~ 4 difference between the bandwidths of the bipolaron on square and triangular lattices. Again, as U decreases there is a remarkable increase in the bandwidth. This effect is not as dramatic as in the case of the square lattice, presumably because the bipolaron already moves with a crablike motion at large U. However the degeneracy between S0 and S1 bipolarons accounts for an additional $\sim 20\%$ increase in the bandwidth, making the bipolarons extra light. This shows how bipolarons can be light over an extremely large regime of the parameter space on triangular lattices.

To highlight the effect of the formation of the hybrid S0-S1 bipolaron on the dispersion, Fig. 20 shows a compari-

son of the variation in the bandwidth as U is changed. The bandwidths of bipolarons on both square and triangular lattices are shown, although it should be noted that the scales are different. There is an increase in bandwidth at $U/W \sim 3$. The widening of the bandwidth is more significant for the square lattice but is also visible for the triangular lattice. The broadening of the bandwidth on the square lattice at intermediate to large U is important, since it shows that light bipolarons are not confined to lattices constructed from triangular plaquettes, but can also exist on simple square, linear, and presumably cubic lattices.

As noted in Sec. I, we can also consider the properties of bipolarons formed from a simplified nearest-neighbor interaction as a means to compare with analytical results. Figure 21 shows the variation in the singlet and triplet dispersions in the near-neighbor model as ω is changed. Bipolarons are considered on both square and triangular lattices with a large electron-phonon coupling of $\lambda=8$. To make comparisons
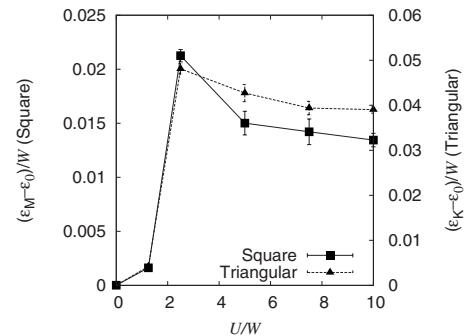

FIG. 20. Light bipolarons at intermediate U/W. The plot shows the variation in the bandwidth with U for the square and triangular lattices. The widening of the bandwidth at intermediate U is more significant for the square lattice but is also visible for the triangular lattice. Parameters for the square lattice are as Fig. 18 and those for the triangular lattice are as Fig. 19 (note that the energies are in terms of W rather than t so that data can be compared more easily).
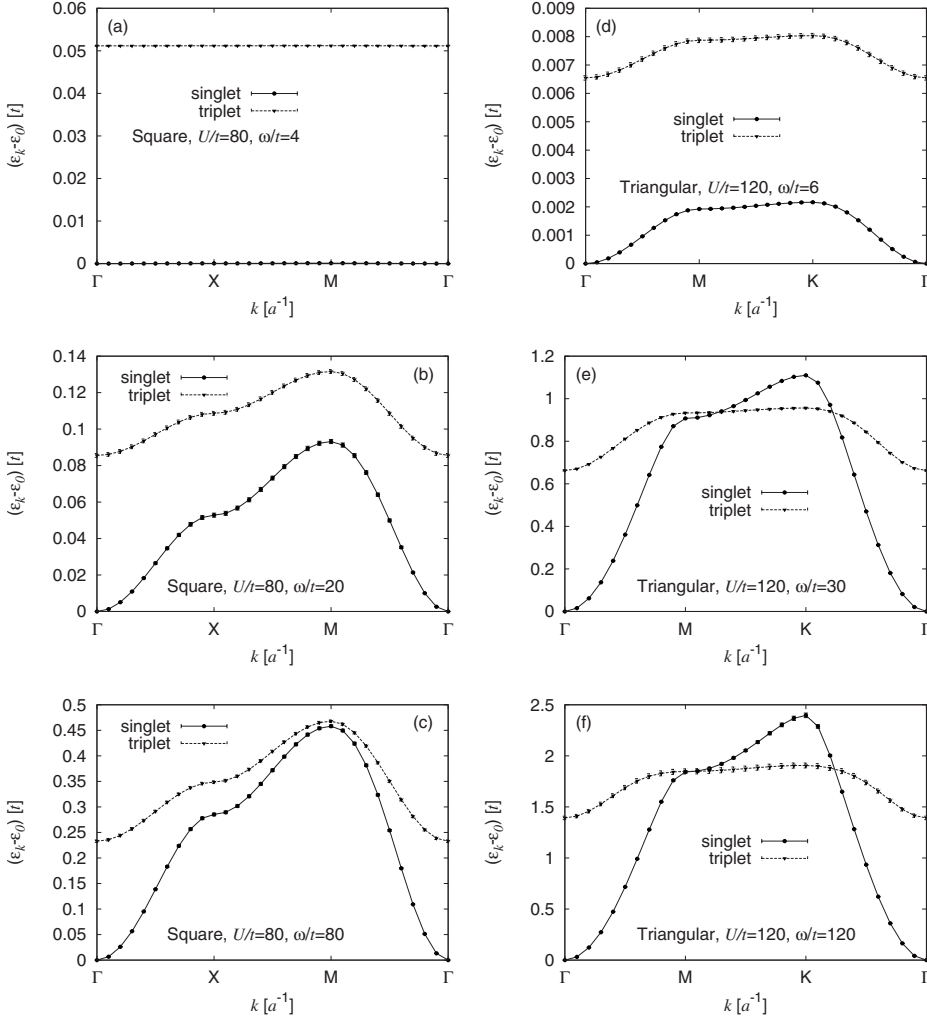
FIG. 21. Stable triplet bipolarons at the Brillouin-zone corner on the triangular lattice. Plots show the variation in singlet and triplet dispersions with frequency with a near-neighbor electron-phonon interaction on square and triangular lattices when $\lambda = 8$ and (c) $\omega = 80t$, square lattice to match with a U-V model with $\bar{U} = 16t$ and $\bar{V} = 32t$, (f) $\omega = 120t$, triangular lattice to match with a U-V model with $\bar{U} = 24t$ and $\bar{V} = 48t$. Also shown for the triangular lattice are $\bar{\omega} = 30$ (panel e) and $\bar{\omega} = 6$ (panel d) and for the square lattice, $\bar{\omega} = 20$ (panel b) and $\bar{\omega} = 4$ (panel a). On the square lattice, $\bar{\beta} = 3.5$ and $U = 80t$ and on the triangular lattice, $\bar{\beta} = 7/3$ and $U = 120t$.

with the UV model, we choose a large phonon frequency $\omega = 120t$ on the triangular lattice (and $\omega = 80t$ on the square lattice). A large Coulomb repulsion of $U = 120t(U = 80t)$ stops on-site pairing, which leads to a U-V model with $\tilde{U} = 24t(\tilde{U} = 16t)$ and $\tilde{V} = 48t(\tilde{V} = 32t)$. We also compute the dispersions of bipolarons on the triangular lattice when $\bar{\omega} = 30$ and $\bar{\omega} = 6$ ($\bar{\omega} = 20$ and $\bar{\omega} = 4$ on the square lattice).

The dispersion of the near-neighbor bipolaron on the triangular lattice at large phonon frequency yields an unusual result. The singlet and triplet bands cross. We note again that the QMC algorithm picks out only the lowest energies associated with singlet and triplet states. In the plot, the s band is visible, along with the lowest p band. A crossing is very unexpected since in all situations that we have previously studied, the triplet band has always sat above the singlet one. This indicates that there will be a transition from singlet to triplet states if sufficient momentum can be imparted to the bipolarons. The crossing remains down to lower phonon frequencies $\hbar\omega \sim 5W$ but is not visible in the adiabatic regime.

In Appendix A, we summarize the analytical approach to solving the UV model on a triangular lattice when pairs have finite momentum and the full dispersion can be seen in Fig. 22. The energy-level crossing is clearly visible, and by comparison it is clear that a single s band and a single p band are visible in Fig. 21. Note that there are a total of six possible

bands associated with the bipolaron, although it is unlikely that the higher energy bands would be excited in any normal transport process.

The band crossing cannot be seen for bipolarons on the square lattice, rather the singlet and triplet pairs become degenerate at the zone edge as the phonon frequency increases. This feature is also visible in the dispersion of bipolarons on the chain[6] and is probably a generic feature of bipolarons on lattices with cubic symmetry.

VII. SUMMARY

In this paper, we computed the properties of bipolarons on two-dimensional lattices using a continuous-time quantum Monte Carlo algorithm. Properties of the bipolaron including the total energy, inverse mass, bipolaron radius, and number of phonons associated with the bipolaron demonstrated the qualitative difference between models of electron-phonon interaction with long-range interaction (screened Fröhlich) and those with purely local (Holstein) interaction, with only small long-range tails needed to completely change the properties of the bipolaron. A major result of our survey of the parameter space is the existence of extra-light hybrid bipolarons consisting of an on-site and an off-site component when on-site and intersite bipolaron configurations are de-
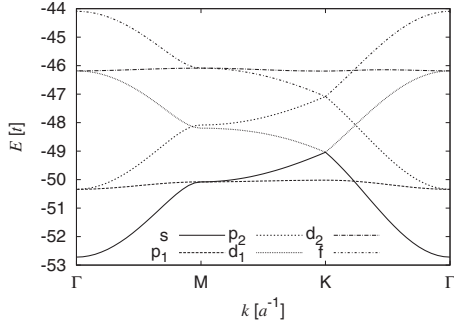
FIG. 22. The spectrum of bound pair in the UV model on the triangular lattice at zero temperature. $U=24t$ and $V=48t$, which corresponds to $\lambda=8$, $U=20W$, and $\omega\rightarrow\infty$. Notice the crossing of the lowest singlet and triplet states near the edge of the Brillouin zone at the M point.

generate, similar to the previously reported superlight bipolarons, but slightly lighter on the triangular lattice, and significantly lighter than the strong coupling intersite bipolarons on the square lattice. We also compute triplet properties of the bipolarons. A major surprise is that triplet pairs with large momentum (close to the K point) are more stable than singlet states on the triangular lattice.

The potential for the existence of local triplet pairs that are preferentially bound could open new avenues in the theory of superconductivity. At low momenta, triplet pairs are necessarily higher in energy than their singlet counterparts since an exact theorem requires the ground-state wave function of a pair to have no nodes. No such theorem exists for states with high pair momentum, however the existence of stable triplet states is unexpected. Thus, in addition to the potential for BCS-BEC crossover as the attractive potential is tuned, there is an additional possibility of triplet BCS to triplet BEC crossover, or even a transition between singlet and triplet pairings. We believe that such a possibility should be investigated further.

Our other finding of light hybrid bipolarons on the square lattice at intermediate coupling and Coulomb repulsion is also significant. While the effect only exists over a very narrow range of coupling constants, it shows that exotic lattice types are not necessary for small light pairs that could have potential to form a Bose condensate with a moderately high transition temperature. This could be of interest to quasi-2D materials that have been suggested to be bipolaron superconductors such as layered bismuthate superconductors (and possibly other superconductors). As in the case of the triangular lattice, light pairs are only a prerequisite for a high-temperature BEC, as other factors such as an absence of clustering in the many particle limit need to be confirmed as part of the scaling needed to understand systems which contain many electrons. Work to discuss this clustering will form the basis of a future publication.

APPENDIX A: UV MODEL ON THE TRIANGULAR LATTICE

The quantum-mechanical problem of two interacting particles on a lattice can be solved exactly as long as the radius of the interaction is finite. Of special interest here is the spectrum of bound pairs that form when at least part of the potential is attractive. The general solution of the bound-state problem results in a spectral equation[30–32] in the form of a determinant with a size equal to the number of lattice sites within the interaction range. For the nonretarded UV model with on-site Hubbard repulsion U and nearest-neighbor attraction $-V$, the determinant is 3×3 for the one-dimensional chain, 5×5 for the square lattice, 7×7 for the triangular lattice, and so on. The subsequent analysis can be simplified by considering the symmetric and antisymmetric states (that is, the singlets and triplets) separately. This effectively halves the number of interaction sites and halves the size of the determinants as a result. For the UV model on the triangular lattice, the size of the singlet determinant reduces to 4 (symmetric combinations of the nearest neighbors plus the central site), and that of the triplet determinant to 3 (antisymmetric combinations of the nearest neighbors).

Omitting the straightforward but lengthy derivation, the spectral equation for the singlet bound pair of the lattice momentum $\mathbf{K}$ is

$$\begin{vmatrix} US_{00}-1 & -VS_{01} & -VS_{02} & -VS_{03} \\ -VS_{10} & -VS_{11}-1 & -VS_{12} & -VS_{13} \\ -VS_{20} & -VS_{21} & -VS_{22}-1 & -VS_{23} \\ -VS_{30} & -VS_{31} & -VS_{32} & -VS_{33}-1 \end{vmatrix}=0, \tag{A1}$$
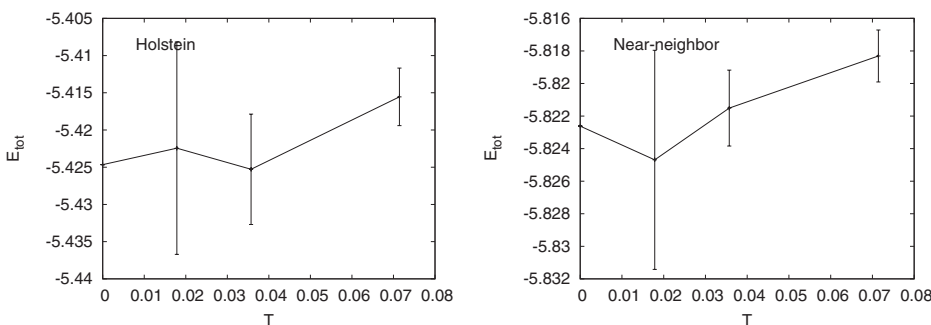
where

FIG. 23. Comparison with the exact results in Ref. 19 for 1D bipolaron models. The points at $T=0$ are the exact results. In the case of near-neighbor interactions, CTQMC attains agreement to better than 0.1% and for the Holstein model, agreement better than 0.3% can be gained during a reasonable run time. Note the temperature corrections for higher T.
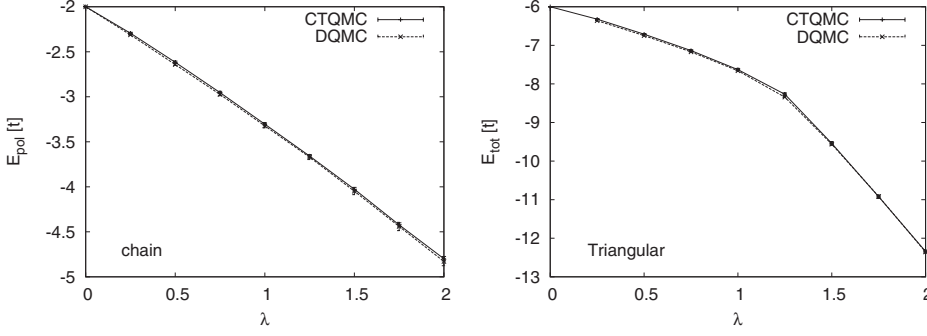
FIG. 24. Comparison between CTQMC ($\beta = 14$) and DQMC ($T=0$). Agreement is found between the two techniques up to a small temperature correction.

$$S_{j0}(\boldsymbol{K}) = \frac{1}{N} \sum_{\boldsymbol{q}} \frac{e^{i\boldsymbol{q}\boldsymbol{n}_j}}{E + \Delta(\boldsymbol{K},\boldsymbol{q})}, \tag{A2}$$

$$S_{jk}(\boldsymbol{K}) = \frac{2}{N} \sum_{\boldsymbol{q}} \frac{e^{i\boldsymbol{q}\boldsymbol{n}_j} \cos(\boldsymbol{q}\boldsymbol{n}_k)}{E + \Delta(\boldsymbol{K},\boldsymbol{q})}, \tag{A3}$$

$$\Delta(\boldsymbol{K},\boldsymbol{q}) = 4t \cos\frac{K_x}{2}\cos q_x + 8t \cos\frac{K_x}{4}\cos\frac{\sqrt{3}K_y}{4}\cos\frac{q_x}{2}\cos\frac{\sqrt{3}q_y}{2}$$

$$+ 8t \sin\frac{K_x}{4}\sin\frac{\sqrt{3}K_y}{4}\sin\frac{q_x}{2}\sin\frac{\sqrt{3}q_y}{2}. \tag{A4}$$

Here the vectors $\boldsymbol{n}_{j,k}$ denote the nearest-neighbor sites of the triangular lattice: $\boldsymbol{n}_0 = (0,0)$; $\boldsymbol{n}_1 = (1,0)$; $\boldsymbol{n}_2 = (\frac{1}{2}, \frac{\sqrt{3}}{2})$; and $\boldsymbol{n}_3 = (-\frac{1}{2}, \frac{\sqrt{3}}{2})$.

Equation (A1) can be solved numerically with respect to the pair energy E for the given pair momentum $\boldsymbol{K}$. For a positive on-site repulsion U and a large enough intersite attraction V, the equation has three roots that we denote s, d_1, and d_2 states. The evolution of the energies as a function of $\boldsymbol{K}$ is shown in Fig. 22 At the high-symmetry points of the Brillouin zone, the system of Eq. (A1) can be further diagonalized into smaller blocks by a proper linear transformation. Thus, at the Γ point $\boldsymbol{K}=(0,0)$, the spectrum splits into the standalone ground state s and a degenerate doublet (d_1,d_2). In the corner of the Brillouin zone, the states s and d_1 become degenerate, as can be seen from Fig. 22.

The triplet bound states can be treated similarly. The exact spectrum equation is a 3×3 determinant,

$$\begin{vmatrix} -VT_{11}-1 & -VT_{12} & -VT_{13} \\ -VT_{21} & -VT_{22}-1 & -VT_{23} \\ -VT_{31} & -VT_{32} & -VT_{33}-1 \end{vmatrix} = 0, \tag{A5}$$

$$T_{jk}(\boldsymbol{K}) = \frac{(-2i)}{N} \sum_{\boldsymbol{q}} \frac{e^{i\boldsymbol{q}\boldsymbol{n}_j} \sin(\boldsymbol{q}\boldsymbol{n}_k)}{E + \Delta(\boldsymbol{K},\boldsymbol{q})} \tag{A6}$$

with the same meaning of $\boldsymbol{n}_{j,k}$ and Δ. The equation does not depend on the on-site repulsion at all, as expected. At the Γ

point, the spectrum splits into a low-energy doublet (p_1,p_2) and a standalone high-energy f state, (see Fig. 22). At the K point, p_2 and f are degenerate.

Two comments are in order. (i) For strongly coupled pairs, the classification of the different orbital states is basically the one of a single particle on a six-site tight-binding ring. (ii) Notice the general property of level crossing between the lowest singlet and triplet states. While the singlet is always the ground state at small momenta, the triplet becomes the lowest state at large momenta. The same property has been observed for the bipolaron, as discussed in the main text of the paper.

APPENDIX B: CODE VALIDATION

We briefly mention additional details providing evidence of the validity of our code. We have compared our code with exactly known results[19] from 1D models: (1) at $\lambda=0.5$, $\omega/t = U/t = 1$, and a near-neighbor interaction, Ref. 19 states the total bipolaron energy as $E_{tot} = -5.822621$ (accurate to seven significant figures) and we compute -5.820 ± 0.0033 at $\beta = 56$ consistent with those values to an accuracy of approximately 0.1%. (2) At $\lambda=0.5$, $\omega/t=1$, and $U/t=0$ for Holstein interaction, Ref. 19 quotes $E_{tot} = -5.4246528$ and we find $E_{tot} = -5.42 \pm 0.014$ (Fig. 23).

In addition, we compare with results for polarons computed using diagrammatic quantum Monte Carlo[20] to simulate the effect of a near-neighbor electron-phonon interaction with $f_{\boldsymbol{n},\boldsymbol{m}} \propto \Sigma_{\boldsymbol{a}_i} \delta_{\boldsymbol{n},\boldsymbol{m}+\boldsymbol{a}_i/2}$—here our code has been used with a separating potential so that our two-particle code can be used to make a comparison with polaron results from DQMC. The results from this comparison can be seen in Fig. 24 for the 1D chain and 2D triangular lattice (by simulating the triangular lattice in this way, triple kink insertions can be checked). The comparison shows exact agreement once temperature corrections are taken into account (our CTQMC code runs as finite temperature while DQMC is a zero-temperature technique). The use of a near-neighbor interaction to make the comparison is useful to test the parts of our code that deal with long-range interaction, which are the same for the lattice Fröhlich interaction.

[1] A. S. Alexandrov and N. Mott, *High Temperature Superconductors and Other Superfluids* (Taylor & Francis, London, 1994).

[2] G. Wellein, H. Röder, and H. Fehske, Phys. Rev. B **53**, 9666 (1996).

[3] A. Weiße, H. Fehske, G. Wellein, and A. R. Bishop, Phys. Rev. B **62**, R747 (2000).

[4] J. Bonča, T. Katrašnik, and S. A. Trugman, Phys. Rev. Lett. **84**, 3153 (2000).

[5] E. Jeckelmann, C. Zhang, and S. R. White, Phys. Rev. B **60**, 7950 (1999).

[6] J. P. Hague and P. E. Kornilovitch, Phys. Rev. B **80**, 054301 (2009).

[7] M. Hohenadler, M. Aichhorn, and W. von der Linden, Phys. Rev. B **71**, 014302 (2005).

[8] M. Hohenadler and W. von der Linden, Phys. Rev. B **71**, 184309 (2005).

[9] L.-C. Ku, S. A. Trugman, and J. Bonča, Phys. Rev. B **65**, 174306 (2002).

[10] A. S. Alexandrov, Phys. Rev. B **53**, 2863 (1996).

[11] A. S. Alexandrov and P. E. Kornilovitch, J. Phys.: Condens. Matter **14**, 5337 (2002).

[12] J. P. Hague, P. E. Kornilovitch, J. H. Samson, and A. S. Alexandrov, Phys. Rev. Lett. **98**, 037002 (2007).

[13] J. P. Hague, P. E. Kornilovitch, J. H. Samson, and A. S. Alexandrov, J. Phys.: Condens. Matter **19**, 255214 (2007).

[14] A. Macridin, G. A. Sawatzky, and M. Jarrell, Phys. Rev. B **69**, 245111 (2004).

[15] A. La Magna and R. Pucci, Phys. Rev. B **55**, 14886 (1997).

[16] G. De Filippis, V. Cataudella, G. Iadonisi, V. Marigliano Ramaglia, C. A. Perroni, and F. Ventriglia, Phys. Rev. B **64**, 155105 (2001).

[17] J. Bonča and S. A. Trugman, Physica C **364-365**, 141 (2001).

[18] The strict analogue of the near-neighbor model would have ions above near-neighbor bonds, which would only interact with electrons at the ends of those bonds. In that case, $\Phi(a)$ $=\Phi(0)/4$ for the square lattice and $\Phi(a)=\Phi(0)/6$ on the triangular lattice.

[19] J. Bonča and S. A. Trugman, Phys. Rev. B **64**, 094507 (2001).

[20] A. S. Mishchenko, N. V. Prokof'ev, A. Sakamoto, and B. V. Svistunov, Phys. Rev. B **62**, 6317 (2000).

[21] J. Bonča and S. A. Trugman, J. Supercond. **13**, 999 (2000).

[22] K. Ishida, H. Mukuda, Y. Kitaoka, K. Asayama, Z. Q. Mao, Y. Mori, and Y. Maeno, Nature (London) **396**, 658 (1998).

[23] K. Ishida, D. Ozaki, T. Kamatsuka, H. Tou, M. Kyogaku, Y. Kitaoka, N. Tateiwa, N. K. Sato, N. Aso, C. Geibel, and F. Steglich, Phys. Rev. Lett. **89**, 037002 (2002).

[24] R. Micnas, J. Ranninger, and S. Robaszkiewicz, Rev. Mod. Phys. **62**, 113 (1990).

[25] P. Nozieres and S. Schmitt-Rink, J. Low Temp. Phys. **59**, 195 (1985).

[26] M. Randeria, N. Trivedi, A. Moreo, and R. T. Scalettar, Phys. Rev. Lett. **69**, 2001 (1992).

[27] P. E. Kornilovitch, Phys. Rev. Lett. **81**, 5382 (1998).

[28] J. P. Hague, P. E. Kornilovitch, A. S. Alexandrov, and J. H. Samson, Phys. Rev. B **73**, 054303 (2006).

[29] We note that strictly the two unbound polarons form a continuum of states relating to the possibility that the momentum was not equally shared between the two particles but that the contribution from the higher energy excitations (i.e., those where the momentum is not split equally between the two particles) is exponentially vanishing as temperature is reduced so that the bottom of the continuum is sampled at the lowest temperatures (with a tiny correction from the excitations) and the results correspond directly to a sum of two polaron dispersions.

[30] P. E. Kornilovitch, *Polarons and Bipolarons in High-T_c Superconductors and Related Materials* (Cambridge University Press, Cambridge, England, 1995), Chap. 23, p. 367.

[31] P. E. Kornilovitch, Ph.D. thesis, King's College London, 1997.

[32] P. E. Kornilovitch, Phys. Rev. B **69**, 235110 (2004).